Unified Modeling and Control of Walking and Running on the Spring-Loaded Inverted Pendulum

Mohammad Shahbazi, *Member, IEEE*, Robert Babuška, *Member, IEEE*, and Gabriel A. D. Lopes, *Member, IEEE*

***Abstract*—This paper addresses the control of steady state and transition behaviors for the bipedal spring-loaded inverted pendulum (SLIP) model. We present an event-driven control approach that enables the realization of active running, walking, and walk–run transitions in a unified framework. The synthesis of the controlled behaviors is illustrated by the notion of hybrid automaton in which different gaits are generated as the sequential composition of SLIP's primary phases of motion. We also propose a novel analytical approximate solution to the otherwise nonintegrable double-stance dynamics of the SLIP model. The analytical simplicity of the solution is utilized in the design and analysis of dynamic walking gaits suitable for online implementation. The accuracy of the approximate solution and its influence on the stability properties of the controlled system are carefully analyzed. Finally, we present two simulation examples. The first demonstrates the practicality of the proposed control strategy in creating human-like gaits and gait transitions. In the second example, we use the controlled SLIP as a planner for the control of a multibody bipedal robot model, and embed SLIP-like behaviors into a physics-based robot simulation model. The results corroborate both the practical utility and effectiveness of the proposed approach.**

***Index Terms*—Double-stance dynamics, legged robots, motion planning and control, spring-mass walking, walk–run transitions.**

I. Introduction

LEGGED animals still outperform man-made locomotory systems equipped with wheels or tracks when it comes to traversing rough and unstructured terrain [1]. This has captured the interest of researchers and engineers in the field of biomechanics and robotics to analyze and design legged systems that are inspired by or mimick nature. Despite significant improvements achieved, there is still much to be done to match the flexibility, agility, and robustness of many land animals and humans. The astonishing specialization, complexity, and performance of the animals' body and brain challenges the current man-made legged morphologies [2].

Manuscript received November 4, 2015; revised May 30, 2016; accepted June 12, 2016. This paper was recommended for publication by Associate Editor P.-B. Wieber and Editor A. Kheddar upon evaluation of the reviewers' comments. The work of M. Shahbazi was supported by the Ministry of Science, Research and Technology of the Islamic Republic of Iran through his scholarship.

M. Shahbazi is with Delft Center for Systems and Control, Delft University of Technology, Delft 2628 CD, the Netherlands, and also with the Department of Mechatronic Systems Engineering, Faculty of New Sciences and Technologies, University of Tehran, Tehran 14399-57131, Iran (e-mail: m.shahbaziaghbelagh@tudelft.nl).

R. Babuška and G. Lopes are with Delft Center for Systems and Control, Delft University of Technology, Delft 2628 CD, the Netherlands (e-mail: r.babuska@tudelft.nl; g.a.delgadolopes@tudelft.nl).

Color versions of one or more of the figures in this paper are available online at http://ieeexplore.ieee.org.

Digital Object Identifier 10.1109/TRO.2016.2593483

Legged locomotion in unstructured terrain is a complex task to be implemented in a system with complex dynamics. To design and analyze such systems, intuitive approaches inspired by biology alone have shown limited success. A deep understanding of the underlying physical principles in locomotion, both at the proprioception level and actuation, enhances the design process, particularly when dynamical, efficient, dexterous, and autonomous platforms are desired. To this end, abstract models capturing the essential characteristics of legged locomotion (namely phase switching) have been established: the inverted pendulum model for walking [3] and the spring-mass model, also referred to as the spring-loaded inverted pendulum (SLIP), for running [4].

Early biomechanical studies [4]–[7] revealed that the SLIP accurately models the center of mass (CoM) dynamics of animals and humans when hopping and running in the sagittal plane. This was observed for a wide range of animals of varying size, as diverse as bipeds, quadrupeds, and animals with more legs, such as cockroaches. In parallel, promising results gained from the design of Raibert's hoppers [8] based on the intuitive exploitation of the SLIP dynamics led to increasing attention in the field of dynamic locomotion. In consequence, a number of successful designs based on this instrumental abstract model were made, most notably the ARL monopods [9], [10], the bow leg hopping robot [11], RHex [12] and its modified versions, BigDog [13], and ATRIAS [14].

Recently, the utility of the spring-mass models was expanded in [15] to represent the walking gait as well. The proposed model consists of a pair of SLIPs forming a bipedal model, which we refer to as the bipedal SLIP. It is shown in [15] that the bipedal SLIP captures the behavioral properties of walking better than the classical inverted pendulum. Additionally, it enables the study of walking and running, the two gaits most commonly used by humans, on the same basis (see, for example, [15]–[17]). Subsequent studies [18], [19] describing the robot dynamics by the bipedal SLIP have reinforced the relevance of this simple model in the design of walking robots.

A number of studies addressing the control of dynamic legged locomotion have used the SLIP as a template [2] for real robots [20]–[25], demonstrating the benefit of the SLIP models, even for legged robots with no SLIP-like morphologies. The general idea is to control the actuated degrees of freedom (DoF) of the real (high dimensional) robot in such a way that it behaves like the template (lower dimensional) model. This can enforce the real robot to mimic the template CoM motion [23], or may utilize the template as a target (i.e., the *hybrid zero dynamics* [26]) for asymptotic behavior of the real robot [20]. In both

cases, there is a continuous coordination between the template model and the controlled system.

The goal of this paper is to develop a controlled SLIP model that performs walking, running, and walk–run transition gaits in *a unified framework*, and to use the developed model as a planner for the control of multibody robot models. We present a hybrid automaton that unifies the representation of walking and running. By following this approach, the hybrid dynamics of the walking, running, and transitions can be partitioned into phases that are well suited for analysis. To create active gaits, we use an event-driven controller to adjust the legs' stiffness. To utilize the analytical simplicity of the SLIP, we use a piecewise constant stiffness profile, in the sense that the changes in the leg stiffness are treated as discrete jumps. When needed, the leg touchdown angle is also controlled to modulate the interchange between kinetic and potential energy.

Creating active dynamic gaits require a deep understanding of the underlying physical principles. Analytical tools play a crucial role here. An explicit time-domain solution of the system dynamics significantly benefits not only the characterization of gaits but also the design of controllers that perform desired motions. The control calculations can hence be executed online, since there would be no numerical integration involved in such a computationally effective solution. Moreover, for some especial cases, it enables the stability of the resulting controlled system to be investigated analytically.

Unfortunately, the exact form of such an instrumental solution of the SLIP stance dynamics is an open problem to date. For the single-stance dynamics, however, several approximate solutions have been studied by linearizing the effect of gravitational force. We introduce a novel approximation for the double-stance dynamics, enabling us to develop a class of controllers that enlarge the domain of system parameters leading to stable walking gaits. The influence of the approximation errors on the stability properties of the resulting controlled system is carefully analyzed. We also use such analytical tools to synthesize controllers that realize walk-to-run transition (WRT) and run-to-walk transition (RWT).

In Section II, after describing the SLIP structure and its mathematical model, we introduce a hybrid automaton representing the walking and running gaits together with their transitions. Then, a discrete abstraction of the system dynamics, namely the return map, is defined both for running and walking gaits. Section III is devoted to the analytical maps representing the system dynamics in the three primary phases of motion: flight, single-stance, and double-stance. In particular, a novel approximate solution to the nonintegrable double-stance dynamics of the bipedal SLIP is detailed, and its prediction accuracy is assessed. Next, in Section IV, we present a number of possible applications to gait control devised on the basis of the analytical maps, including the synthesis of controllers that realize the WRT and RWT. This is followed by a simulation study in Section V, in which we give two example applications of the proposed control strategies: one focusing on the simulation of human-like walking and running on the SLIP model and the other demonstrating the usefulness of the results in the control of multibody walking robot models.

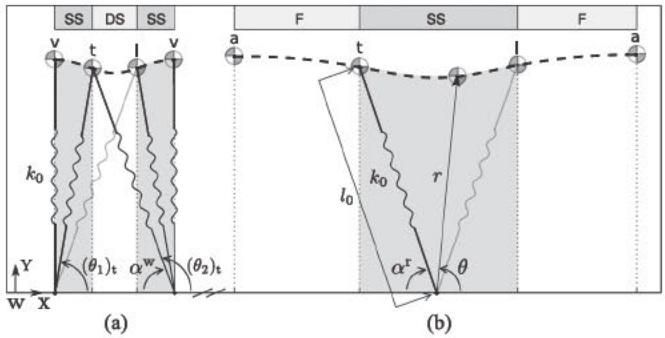

Fig. 1. Bipedal SLIP model in (a) walking and (b) running gaits. See Table I for the notation. The corresponding single-stance phases are shaded in both gaits.

TABLE I
NOTATION USED TO DEFINE THE SLIP HYBRID AUTOMATON

	gait		phase
r	running	F	flight
w	walking	SS	single-stance
rw	run-to-walk transition	DS	double-stance
wr	walk-to-run transition		**event**
		a	apex
	subphase	b	bottom
sc	spring compression	v	VLO
sd	spring decompression	$\tilde{b}$	virtual bottom
ba	before VLO	t	touchdown
aa	after VLO	l	liftoff
ba	before apex	f	front leg liftoff
aa	after apex	r	rear leg liftoff

Some of the ideas in Sections III-C and IV-C were previously presented in [27] and [28]. However, here we improved the synthesis of WRT controller to fit it with the proposed unified framework, provided an energy-based analysis, developed an algorithmic representation for the derived approximate map, and analyzed the corresponding approximation errors for the entire walking gait by exploring their relation to the Poincaré map.

II. SPRING-LOADED INVERTED PENDULUM

A. Spring-Loaded Inverted Pendulum Model and its Dynamics

The bipedal SLIP model in the walking and running gaits is illustrated in Fig. 1(a) and (b), respectively (see Table I for the general notation used in this paper). The body is represented as a point mass m at the CoM that is connected to two massless springy legs, moving in the sagittal plane with gravitational acceleration g. The legs are represented by linear lossless springs with the nominal constant k_0 and rest length l_0. The system motion is measured with respect to the fixed frame W, as depicted in Fig. 1. It is convenient to further define polar coordinates (r, θ) at the toe position. Notice the difference between $(\theta_i)_t, i \in \{1, 2\}$, which is the ith leg angular position in polar coordinates (r, θ)

at touchdown (t), and $\alpha^{\beta}, \beta \in \{\mathrm{r}, \mathrm{w}\}$, which is the touchdown angle ($\alpha^{\beta} = \pi - (\theta_i)_{\mathrm{t}}$).

To simplify the following study, we assume a point foot, thereby no actuation at the toe position is permitted. We also ignore the effect of the toe impact, and assume that the toe position remains fixed during stance (no slipping). Moreover, we assume no physical meaning for the swing leg, thereby ignoring foot scuffing.

In general, the continuous and discrete state vector of the system in the Cartesian coordinates (x, y) can be expressed as $\mathcal{S} = [\,x \;\; \dot{x} \;\; y \;\; \dot{y}\,]^T$ and $\mathcal{Q} = [\,c_1 \;\; c_2 \;\; \alpha^{\beta} \;\; \mathcal{M}\,]^T$, respectively, where c_1 and c_2 denote the toe positions (these are constant for the duration of the stance phases), and $\mathcal{M} \in \{\mathrm{F}, \mathrm{SS}, \mathrm{DS}\}$ denote the phase of motion, as defined in the following. Depending on how the springs act on the body, three primary phases can be distinguished: flight (F), single-stance (SS), and double-stance (DS). As no spring acts on the body in the F phase, the system is driven by gravity, showing a ballistic trajectory. The system undergoes oscillatory motions in the SS and DS phases due to the influence of a single and double spring, respectively, interacting with gravity. The equations describing the CoM motion in Cartesian coordinates (x, y) are written as

1) F

$$\begin{bmatrix} m\ddot{x} \\ m\ddot{y} \end{bmatrix} = \begin{bmatrix} 0 \\ -mg \end{bmatrix} \tag{1}$$

2) SS

$$\begin{bmatrix} m\ddot{x} \\ m\ddot{y} \end{bmatrix} = \begin{bmatrix} 0 \\ -mg \end{bmatrix} + T_{\mathrm{SS}_i}(x, y) F_{\mathrm{l}_i}(x, y), \quad i \in \{1, 2\} \tag{2}$$

3) DS

$$\begin{bmatrix} m\ddot{x} \\ m\ddot{y} \end{bmatrix} = \begin{bmatrix} 0 \\ -mg \end{bmatrix} + T_{\mathrm{DS}}(x, y) \begin{bmatrix} F_{\mathrm{l}_1}(x, y) \\ F_{\mathrm{l}_2}(x, y) \end{bmatrix} \tag{3}$$

where T_{SS_i}, $i \in \{1, 2\}$, and T_{DS} are transformation matrices and F_{l_i}, $i \in \{1, 2\}$, is the ith leg spring force. See the Appendix for the corresponding expressions.

In the running gait, the system alternates between the F and SS phases. Two important events define the phase transitions: *touchdown* and *liftoff*. The touchdown event occurs when the fully stretched leg touches the ground (assuming flat terrain) with touchdown angle α^{r}, and the leg lifts off the ground when it is fully stretched (i.e., reaches its rest length) in the spring decompression. A single running step starts at the highest vertical position of the CoM in the F phase, called the *apex* and ends at the subsequent apex. We further divide the SS phase into the spring compression and decompression subphases. The *bottom* event, where the spring is at its minimum length, triggers the transition from the compression to decompression subphases.

In the walking gait, the system alternates between the SS and DS phases. Here, the front leg touchdown and the rear leg liftoff define the phase transitions. The system switches from SS to DS when the fully stretched leg touches the ground making α^{w} as the touchdown angle, and switches back to the next SS when the rear leg is fully stretched. A single walking step starts at the *vertical leg orientation (VLO)* in the SS phase, and ends at the subsequent VLO. Similarly to the running gait, we further divide the DS phase into the "virtual" compression and decompression subphases. The corresponding transitions between these two are defined by the so-called *virtual bottom* event. The virtual bottom is the point where the CoM has the minimum distance from the midstance of the legs' toe.[1] We explain in Section IV-B why the virtual bottom is of interest.

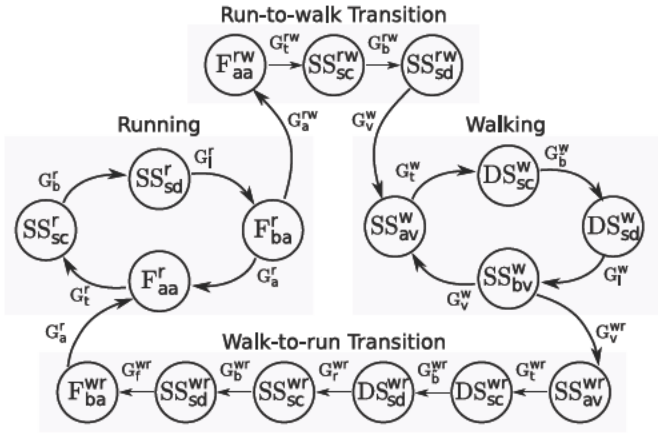

Fig. 2. Hybrid automaton representing the pattern of walking, running, and walk–run transitions in the SLIP model. See Table I for the notation.

B. Hybrid Automaton

As described in the previous section, each walking and running cycle comprises a sequence of different modes with different dynamics, and the switching between the modes is governed by discrete events (transition guards). This means that the SLIP model is hybrid. A number of representations have been proposed for the modeling and analysis of hybrid systems, including the hybrid automaton framework [29]. Fig. 2 depicts the suggested hybrid automaton that represents the controlled SLIP system in walking, running, and walk–run transitions. Every single node, depicted by a circle, represents the system in a particular phase, during which the system parameters, including the legs' stiffness, are kept constant. The notation used to represent a particular node is

$$\mathrm{phase}^{\mathrm{gait}}_{\mathrm{subphase}}.$$

For the transition guards, we use the following notation:

$$\mathrm{G}^{\mathrm{gait}}_{\mathrm{event}}.$$

Associated with each stance mode, the legs' stiffness are represented as

$$k^{\mathrm{gait}}_{\mathrm{subphase}}.$$

[1]The SLIP walker can experience multiple virtual bottom events. In this paper, we focus on the human-like walking patterns (i.e., with the vertical ground reaction forces having an *M*-shape profile), and therefore a single virtual bottom can be experienced.

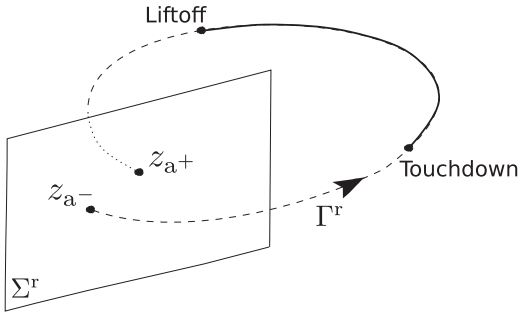

Fig. 3. Abstract view of the Poincaré section taken at apex for the running gait.

Finally, the system states at any particular event take the following form:

$$\mathcal{S}_{\text{event}}.$$

Table I details all the notation that can be used in the possible combinations of these symbols. For instance, $\mathrm{SS}^{\mathrm{w}}_{\mathrm{bv}}$ denotes the SS phase before VLO in the walking gait, and $\mathrm{G}^{\mathrm{r}}_{\mathrm{l}}$ denotes the transition guard due to the liftoff event in the running gait.

Following the definition of the hybrid automaton, a number of reset maps are defined as follows. Whenever the system transitions to SS or DS mode, the leg(s) stiffness is set to the value commanded by a controller; at the touchdown instant, the toe position is reset such that the fully stretched leg makes an angle with the horizontal corresponding to the touchdown angle. The control system also updates the touchdown angle in each cycle once needed.

C. Return Maps

The Poincaré map is a commonly used tool for the analysis of periodic systems, such as the SLIP model in walking and running, which reduces the dimension of the system state via a discrete task-space abstraction in the Poincaré section. For the running gait, we take the Poincaré section at apex [30] by defining the transversal Σ^{r} to the orbit Γ^{r} (see Fig. 3). The reduced system state at this section (z_{a}) contains only two variables

$$z_{\mathrm{a}} = \begin{bmatrix} \dot{x}_{\mathrm{a}} & y_{\mathrm{a}} \end{bmatrix}^T, \quad z_{\mathrm{a}} \in \Sigma^{\mathrm{r}} \subset \mathbb{R}^2. \tag{4}$$

We do not include the CoM horizontal position (x_{a}) in z_{a} because it has no influence on the system dynamics at the Poincaré section from one return to another, when traversing a flat surface; however, we do keep track of it within each locomotion step because of the toes' position and the transition guards. Moreover, the definition of the apex point requires $\dot{y}_{\mathrm{a}} = 0$. Note that the dimension of Σ^{r} can be further reduced to one, if the total energy is conserved. However, we keep it in the general form (two dimensional) to avoid confusion in nonenergy conservative cases, such as active gaits.

Accordingly, the apex return map (ARM) $\mathcal{P}^{\mathrm{r}} : \Sigma^{\mathrm{r}} \to \Sigma^{\mathrm{r}}$ gives a mapping between two subsequent apex states in Σ^{r} as

$$z_{\mathrm{a}^+} = \mathcal{P}^{\mathrm{r}}(z_{\mathrm{a}^-}). \tag{5}$$

Following the definition of the phases in Fig. 1(b), the ARM can be constructed by composing four subsequent maps: the apex to touchdown (${}^{\mathrm{t}}_{\mathrm{a}^-}\mathcal{P}^{\mathrm{r}}$), the touchdown to bottom (${}^{\mathrm{b}}_{\mathrm{t}}\mathcal{P}^{\mathrm{r}}$), the bottom to liftoff (${}^{\mathrm{l}}_{\mathrm{b}}\mathcal{P}^{\mathrm{r}}$), and the liftoff to apex (${}^{\mathrm{a}^+}_{\mathrm{l}}\mathcal{P}^{\mathrm{r}}$). The ARM (5) therefore takes the following form:

$$z_{\mathrm{a}^+} = \left({}^{\mathrm{a}^+}_{\mathrm{l}}\mathcal{P}^{\mathrm{r}} \circ {}^{\mathrm{l}}_{\mathrm{b}}\mathcal{P}^{\mathrm{r}} \circ {}^{\mathrm{b}}_{\mathrm{t}}\mathcal{P}^{\mathrm{r}} \circ {}^{\mathrm{t}}_{\mathrm{a}^-}\mathcal{P}^{\mathrm{r}}\right)(z_{\mathrm{a}^-}). \tag{6}$$

For the walking gait, we take the Poincaré section at VLO [16]. Following a similar process as for running, the transversal $\Sigma^{\mathrm{w}} \subset \mathbb{R}^3$ to the orbit Γ^{w} is defined, and the VLO return map (VRM) $\mathcal{P}^{\mathrm{w}} : \Sigma^{\mathrm{w}} \to \Sigma^{\mathrm{w}}$ defines a mapping between two subsequent VLO states in Σ^{w}

$$z_{\mathrm{v}^+} = \mathcal{P}^{\mathrm{w}}(z_{\mathrm{v}^-}) \tag{7}$$

where the VLO state in Σ^{w} takes the form

$$z_{\mathrm{v}} = \begin{bmatrix} \dot{x}_{\mathrm{v}} & y_{\mathrm{v}} & \dot{y}_{\mathrm{v}} \end{bmatrix}^T, \quad z_{\mathrm{v}} \in \Sigma^{\mathrm{w}}. \tag{8}$$

Here, the definition of the VLO state already implies the horizontal position (x_{v}). The VRM is the composition of four maps: the VLO to touchdown (${}^{\mathrm{t}}_{\mathrm{v}^-}\mathcal{P}^{\mathrm{w}}$), the touchdown to virtual bottom (${}^{\tilde{\mathrm{b}}}_{\mathrm{t}}\mathcal{P}^{\mathrm{w}}$), the virtual bottom to liftoff (${}^{\mathrm{l}}_{\tilde{\mathrm{b}}}\mathcal{P}^{\mathrm{w}}$), and the liftoff to VLO (${}^{\mathrm{v}^+}_{\mathrm{l}}\mathcal{P}^{\mathrm{w}}$), as illustrated in Fig. 1(a)

$$z_{\mathrm{v}^+} = \left({}^{\mathrm{v}^+}_{\mathrm{l}}\mathcal{P}^{\mathrm{w}} \circ {}^{\mathrm{l}}_{\tilde{\mathrm{b}}}\mathcal{P}^{\mathrm{w}} \circ {}^{\tilde{\mathrm{b}}}_{\mathrm{t}}\mathcal{P}^{\mathrm{w}} \circ {}^{\mathrm{t}}_{\mathrm{v}^-}\mathcal{P}^{\mathrm{w}}\right)(z_{\mathrm{v}^-}). \tag{9}$$

The ARM and VRM, formulated in (6) and (9), are effective representations for the SLIP dynamics in running and walking that can be utilized for the stability and control purposes.

III. Analytical Maps

Toward the design of controllers that are computationally efficient for online implementation, in this section, we seek analytical time solutions to the SLIP dynamics, allowing the construction of the ARM and VRM. As will be shown for the stance phases, this can be constituted only in approximate forms. Therefore, a characterization of the propagated errors due to approximations is also presented.

A. Flight Map

Integrating the flight dynamics expressed by (1) results in the following well-known expressions for the movement of the CoM:

$$\begin{bmatrix} \dot{x} \\ \dot{y} \end{bmatrix} = \begin{bmatrix} \dot{x}_0 \\ -gt + \dot{y}_0 \end{bmatrix}, \quad \begin{bmatrix} x \\ y \end{bmatrix} = \begin{bmatrix} \dot{x}_0 t + x_0 \\ -gt^2/2 + \dot{y}_0 t + y_0 \end{bmatrix} \tag{10}$$

where $(\cdot)_0$ denotes the initial value at time $t = 0$. The submaps ${}^{\mathrm{t}}_{\mathrm{a}^-}\mathcal{P}^{\mathrm{r}}$ and ${}^{\mathrm{a}^+}_{\mathrm{l}}\mathcal{P}^{\mathrm{r}}$ can be determined using (10).

B. Single-Stance Map

The simplicity of the physical structure of the SLIP model seemingly suggests that deriving a closed-form solution to its dynamics in the stance phases is simple as well. However, such an analytical solution has remained an open problem to date. It has been shown that the mentioned dynamics under the influence of gravity are nonintegrable [31], [32]. Lacking such a closed-form representation has limited the use of functional analysis tools, which could be instrumental in the design of

dexterous and dynamic legged robots. If an arbitrarily close approximation to the exact solution of the SLIP dynamics is to be predicted, then the common approach is through relatively extensive forward-in-time numerical integrations (e.g., [33]–[35]), where the tradeoff between precision and computational complexity plays an important role. As such, precise numerical approximations might not be suitable for online implementation. Moreover, the numerical nature of such solutions precludes the possibility of deriving a closed-form expression for the associated Jacobian matrix.

Nevertheless, several alternatives aiming at finding an accurate analytical approximation to the SLIP dynamics in the SS phase have been proposed [36]–[40], which rely on simplified and linearized dynamic models. The approximation presented in [37] ignores the effect of gravity in stance, something that can hardly be fulfilled in reality. Geyer *et al*. [38] proposed a simple solution, in terms of elementary functions, that approximates the ARM without the need for an iterative process. The simplicity of the solution is such that it can further be used to investigate the stability of ARMs in some special situations. Although the method takes into account a linearized effect of gravity in the force balance equations, it presumes the conservation of angular momentum, an assumption that can significantly be violated in nonsymmetric gaits[2] due to gravity. Using an iterative algorithm based on the mean-value theorem, Schwind and Koditschek [36] proposed another noteworthy approximation. The main characteristic of their method is its iterative form, in the sense that at least two iterations are required in order to meet a minimal accuracy threshold. Although the quality of the results increasingly improves with each iteration, the mathematical complexity of the resulting solution negatively affects the utility of the method for further usage, such as stability analysis.

Inspired by this work, Arslan *et al.* [41] expanded the Geyer *et al.* method by adding a gravity correction-based iteration, forming a two-step iterative solution. The method has been further expanded in [42] to handle energy-dissipative elements and the results have been experimentally validated in [43] recently. Subsequent controller designs [42], [44], [45] carried out using this approximation have shown promising results.

Recently, based on the perturbation theory, another solution has been proposed in [40]. The method assumes the angular momentum as a conserved quantity in the radial motion as in the Geyer *et al*. method. However, for the angular motion, the effect of gravitational torque is included leading to a varying angular momentum. The resulting equations are then solved using standard perturbation techniques.

We have found that, among the methods addressed above, the Geyer *et al*. method with the Arslan *et al*. extension suits our scheme. The novel DS approximate map presented in this paper finds its origin in these works. The reminder of this section briefly presents them.

1) Approximate Single-Stance Map by Geyer et al.: In [38], Geyer *et al*. derived a simple solution to the stance phase of the SLIP hopper. The approximation relies on two assumptions: 1) the angle swept during the stance ($\Delta\theta$) is sufficiently small, and the stance phase is predominantly vertical (i.e., $\sin\theta \approx 1$); and 2) the compression of the leg is much smaller than its rest length. Combined with further simplifications detailed in [38], the following expressions for the radial and angular motions of the CoM in polar coordinates (r, θ) are derived[3]:

$$\begin{aligned} r(t) &= \frac{f}{\hat{\omega}_0^2} + \lambda_1 \sin\hat{\omega}_0 t + \lambda_2 \cos\hat{\omega}_0 t \\ \theta(t) &= \frac{2g/l_0 + \omega_0^2 + \omega^2}{\hat{\omega}_0^2}\,\omega t \\ &\quad + \frac{2\omega}{l_0\hat{\omega}_0}(\lambda_1 \cos\hat{\omega}_0 t - \lambda_2 \sin\hat{\omega}_0 t) + \lambda_3 \end{aligned} \tag{11}$$

where $\hat{\omega}_0^2 = \omega_0^2 + 3\omega^2$, $f = -g + l_0\omega_0^2 + 4l_0\omega^2$, $\omega = p/(ml_0{}^2)$, and $\omega_0^2 = k/m$ with $p = mr^2\dot{\theta}$ being the angular momentum of mass m around the toe conserved during motion, which can be substituted by the known angular momentum at the initial condition $p_0 = mr_0^2\dot{\theta}_0$. Finally, λ_1, λ_2, and λ_3 are constant values determined by the initial conditions. This approximate solution is valid for any pair of initial and final conditions within the SS phase, including the touchdown and liftoff points.

2) Gravity Correction Scheme by Arslan et al.: The above-presented method fails when the stance trajectory is nonsymmetric because, in this case, the average angular momentum due to gravity is nonzero, thereby the total angular momentum can no longer be assumed conserved. Motivated by this, Arslan *et al*. [41] have incorporated an average effect of gravity on the angular momentum, which can be approximately modeled as

$$\bar{p}_{\mathrm{g}} = -\frac{t_{\mathrm{e}}}{2} mg\bar{r}(\cos\theta_0 + \cos\theta_{\mathrm{e}}) \tag{12}$$

where subscript "e" stands for the end state, and $\bar{r}$ is the approximated average leg length that can be obtained using (11)

$$\begin{aligned} \bar{r} &= \frac{1}{t_{\mathrm{e}}}\int_0^{t_{\mathrm{e}}} r(t)\,\mathrm{d}t \\ &= \frac{f}{\hat{\omega}_0^2} + \frac{1}{\hat{\omega}_0 t_{\mathrm{e}}}(\lambda_1 - \lambda_1\cos\hat{\omega}_0 t_{\mathrm{e}} + \lambda_2 \sin\hat{\omega}_0 t_{\mathrm{e}}). \end{aligned} \tag{13}$$

Now, the gravity correction term $\bar{p}_{\mathrm{g}}$ is added to the original angular momentum p_0 to yield the updated angular momentum

$$\hat{p} = p_0 + \bar{p}_{\mathrm{g}}. \tag{14}$$

Finally, $\hat{p}$ replaces p_0 in all corresponding derivations, which gives a two-iteration form to the solution.

The presented method effectively establishes an analytical solution to the SS dynamics of the SLIP from any initial to any final state. The maps ${}^{\mathrm{b}}_{\mathrm{t}}\mathcal{P}^{\mathrm{r}}$, ${}^{\mathrm{l}}_{\mathrm{b}}\mathcal{P}^{\mathrm{r}}$, ${}^{\mathrm{t}}_{\mathrm{v}^-}\mathcal{P}^{\mathrm{w}}$, and ${}^{\mathrm{v}^+}_{\mathrm{l}}\mathcal{P}^{\mathrm{w}}$ can be constructed accordingly.

C. Double-Stance Map

In this section, we introduce an approximate time solution to the DS dynamics of SLIP. We define an auxiliary system referred to as the axial-torsional SLIP (AT-SLIP) (see Fig. 4),

[2]In a symmetric gait, the trajectory is symmetric with respect to the VLO.

[3]The instant of the initial condition is defined as $t = 0$.

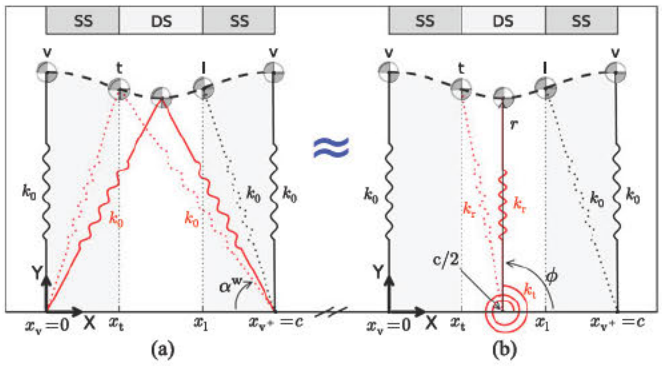

Fig. 4. (a) SLIP model in walking and (b) DS phase of the bipedal SLIP is replaced by an auxiliary system called AT-SLIP, which incorporates an axial and a torsional spring. See Table I for the notation used in the figure.

which under specific assumptions detailed below approximates the CoM trajectories of the bipedal SLIP in the DS phase. The significance of this model is in admitting an approximate analytical solution that can also be qualified as a solution for the original SLIP.

1) Axial-Torsional Spring-Loaded Inverted Pendulum Model: As shown in Fig. 4, the AT-SLIP model consists of a point mass m attached to a *single* spring-loaded leg with spring constant k_r. The toe is located at the midstance of the two original legs, and a torsional spring with constant k_t is added at the same position. The rest length of the axial spring and the zero torque angle of the torsional spring are denoted by l_{r_0} and ϕ_0, respectively. The equations of motion for the AT-SLIP model in Cartesian coordinates x, y are as follows:

$$m\begin{bmatrix}\ddot{x}\\ \ddot{y}\end{bmatrix} = m\begin{bmatrix}0\\ -g\end{bmatrix} + T_{\mathrm{AT}}(x,y)\begin{bmatrix}F_\mathrm{r}(x,y)\\ F_\mathrm{t}(x,y)\end{bmatrix} \tag{15}$$

where T_{AT} is a transformation matrix, F_r is the axial spring force exerted on the mass, and F_t is the resultant force exerted on the mass due to the torque generated by the torsional spring. The corresponding expressions are given in the Appendix.

We find a set of parameters $(k_\mathrm{r}, k_\mathrm{t}, l_{\mathrm{r}_0}, \phi_0)$ for which, under the same initial conditions, the AT-SLIP trajectories approximately coincide with those of the bipedal SLIP in DS, provided that the following assumptions hold:

$$\begin{aligned}&(\Delta l_\mathrm{r})_{\max} \ll l_{\mathrm{r}_0}\\ &\Delta\phi \approx 0 \ \text{ and } \ \sin\phi \approx 1\end{aligned} \tag{16}$$

where $(\Delta l_\mathrm{r})_{\max}$ and l_{r_0} are the maximum compression and the rest length of the axial spring, respectively, and $\Delta\phi$ is the angle swept by the AT-SLIP leg. These assumptions are similar to those made by Geyer *et al.* in [38]. To make the bipedal SLIP in DS (3) and AT-SLIP (15) equivalent systems, the resultant forces on the mass at any arbitrary state, including the equilibrium point, must be the same. We first calculate the equilibrium point of the bipedal SLIP by equating (3) to zero. By symmetry, it immediately follows that $x_{\mathrm{eq}} = c/2$, where the subscript "eq" stands for the *equilibrium* point, and c is the step length. This, in turn, sets

$$\phi_0 = \pi/2. \tag{17}$$

To obtain the legs' length at the equilibrium position (l_{eq}), a simple manipulation of the force balance relation in the vertical direction yields:

$$\begin{aligned}l_{\mathrm{eq}}^4 - 2\,l_0 l_{\mathrm{eq}}^3 + (l_0^2 - c^2/4 - (mg/k_0)^2/4) l_{\mathrm{eq}}^2\\ + c^2/2\,l_0 l_{\mathrm{eq}} - c^2/4\,l_0^2 = 0.\end{aligned} \tag{18}$$

The relevant solution l_{eq} of this polynomial is used to obtain the equilibrium height

$$y_{\mathrm{eq}} = \sqrt{l_{\mathrm{eq}}^2 - c^2/4}. \tag{19}$$

Since the equilibrium point in the two systems should be the same, y_{eq} is used to establish a relation between the axial spring constant and rest length in the AT-SLIP system as

$$l_{\mathrm{r}_0} = \frac{mg}{k_\mathrm{r}} + y_{\mathrm{eq}}. \tag{20}$$

Next, we equate (3) to (15), leading to

$$T_{\mathrm{DS}}(x,y)\begin{bmatrix}F_{\mathrm{l}_1}(x,y)\\ F_{\mathrm{l}_2}(x,y)\end{bmatrix} = T_{\mathrm{AT}}(x,y)\begin{bmatrix}F_\mathrm{r}(x,y)\\ F_\mathrm{t}(x,y)\end{bmatrix}. \tag{21}$$

Solving (21) for k_r and k_t with using (20) in the corresponding terms results in

$$\begin{bmatrix}k_\mathrm{r}(x,y)\\ k_\mathrm{t}(x,y)\end{bmatrix} = A^{-1}B. \tag{22}$$

Matrices A and B are given in the Appendix. The resulting stiffness varies across any arbitrary range of motion. However, by numerical analysis, it can be shown that if assumptions (16) hold, $k_\mathrm{r}(x,y)$ and $k_\mathrm{t}(x,y)$ can be roughly quantified with some limit values $\bar{k}_\mathrm{r}$ and $\bar{k}_\mathrm{t}$, respectively. Mathematically speaking, we first derive a closed-form solution for $\bar{k}_\mathrm{r}$

$$\bar{k}_\mathrm{r} = \lim_{(x,y)\to(c/2,l_{\mathrm{r}_0})} k_\mathrm{r}(x,y) = \frac{mg}{\sqrt{l_0^2 - c^2/4} - y_{\mathrm{eq}}}. \tag{23}$$

Note that we evaluate the limit when (x,y) converge to $(c/2, l_{\mathrm{r}_0})$ as this point best satisfies assumptions (16). Furthermore, we must take the limit rather than simple substitution because the latter results in an indeterminate expression. Also note that since l_{r_0}, as defined in (20), is a function of k_r, replacing y by l_{r_0} in (23) results in an implicit equation in terms of $\bar{k}_\mathrm{r}$, which is straightforward to solve. Next, the derived $\bar{k}_\mathrm{r}$ is substituted in (20) to yield an approximate expression for the rest length of the axial spring

$$\bar{l}_{\mathrm{r}_0} = \frac{mg}{\bar{k}_\mathrm{r}} + y_{\mathrm{eq}}. \tag{24}$$

Finally, we derive a simple expression approximating a constant value for the torsional spring stiffness

$$\bar{k}_\mathrm{t} = \lim_{(x,y)\to(c/2,\bar{l}_{\mathrm{r}_0})} k_\mathrm{t}(x,y) = \frac{4\,k_0 c^2 l_0 \bar{l}_{\mathrm{r}_0}^2}{(c^2 + 4\,\bar{l}_{\mathrm{r}_0}^2)^{3/2}}. \tag{25}$$

In summary, for the set of parameters ($\bar{k}_\mathrm{r}, \bar{k}_\mathrm{t}, \bar{l}_{\mathrm{r}_0}$, and ϕ_0), we derived expressions (23), (25), (24), and (17), respectively, with which the AT-SLIP system (15) approximates the DS dynamics of the bipedal SLIP system (3), provided that assumptions (16) hold.

2) Axial-Torsional Spring-Loaded Inverted Pendulum Dynamics Approximation: In the absence of the torsional spring, the AT-SLIP model would be identical to the original SLIP in SS phase, for which approximate time solutions were reported in Section III-B. All that is needed to complete the time solution of the AT-SLIP dynamics is to find a way to include the effect of the torsional spring, which is present on the angular momentum of the system. We model this effect as

$$p_{\mathrm{t}} = \int_0^{t_{\mathrm{e}}} \bar{k}_{\mathrm{t}} \big(\phi_0 - \phi(t)\big)\, \mathrm{d}t \tag{26}$$

where the integrand is the torque generated by the torsional spring. Substituting $\phi(t)$ from (11)[4] and computing the integral symbolically yields

$$\begin{aligned} p_{\mathrm{t}} = & -\bar{k}_{\mathrm{t}}\omega \left(\frac{2\, g/\bar{l}_{\mathrm{r}_0} + \omega_0^2 + \omega^2}{2\, hat\omega_0^2} t_{\mathrm{e}}^2 + \frac{\lambda_3 - \phi_0}{\omega} t_{\mathrm{e}} \right. \\ & \left. + \frac{2}{\bar{l}_{\mathrm{r}_0}\hat{\omega}_0^2} \left(\lambda_1 \sin\hat{\omega}_0 t_{\mathrm{e}} - \lambda_2 (1 - \cos\hat{\omega}_0 t_{\mathrm{e}})\right) \right). \end{aligned} \tag{27}$$

Now, if one adds p_{t} to the updated angular momentum formulated in (14)

$$\hat{p} = p_0 + \bar{p}_{\mathrm{g}} + p_{\mathrm{t}} \tag{28}$$

and updates all the corresponding derivations accordingly, an approximate solution for the AT-SLIP dynamics is established. This result can also be considered as an approximate time solution of the DS dynamics of the SLIP.

It should be noticed that although using the two-iteration scheme presented above enables us to include the effects of gravity and torsional spring, it causes a loss of continuity of the angular momentum at the start point. More specifically, the angular momentum at the start point is different from what is assigned by the initial condition. However, the difference is so small in the sense of approximation, and it can be safely ignored in practice.

3) Overview of the Double-Stance Map Approximation: To implement the approximation proposed in the previous section, it is sufficient to follow Algorithm 1, which describes the required steps in detail. This algorithm establishes a mapping between any start and end state in the DS phase of the SLIP model. The maps ${}^{\bar{\mathrm{b}}}_{\mathrm{t}}\mathcal{P}^{\mathrm{w}}$ and ${}^{\mathrm{l}}_{\bar{\mathrm{b}}}\mathcal{P}^{\mathrm{w}}$ can be constructed accordingly.

D. Characterization of Approximation Errors

Since the class of controllers presented in the next section is based on the presented approximations, it is important to understand the magnitude of the errors due to approximations. To do so, we consider a sufficiently wide range of initial conditions and system parameters and compare the "exact" (numerical) solutions (ground truth data) to those obtained using the approximate maps. It is sufficient to analyze the approximation error in the walking gait since it encompasses both the SS and DS phases. See [28] for a detailed error analysis of the DS phase alone.

[4]Here $\phi(t)$ replaces $\theta(t)$ due to the different notation for the AT-SLIP system.

Algorithm 1: Approximate solution for the DS dynamics of the bipedal SLIP model.

Inputs: Initial condition, t_{e}, c
1) compute l_{eq} using (18)
2) compute y_{eq} using (19)
3) compute $\bar{k}_{\mathrm{r}}$ using (23)
4) compute $\bar{l}_{\mathrm{r}_0}$ using (24)
5) compute $\bar{k}_{\mathrm{t}}$ using (25)
6) $\phi_0 \leftarrow \pi/2$
7) apply transformation from Cartesian to polar coordinates
8) $\omega_0 \leftarrow \sqrt{\bar{k}_{\mathrm{r}}/m}$
9) $p_0 \leftarrow m r_0^2 \dot{\phi}_0$
10) $\omega \leftarrow p_0/(m\bar{l}_{\mathrm{r}_0}^2)$
11) $\hat{\omega}_0 \leftarrow \sqrt{\omega_0^2 + 3\omega^2}$
12) $F \leftarrow -g + \bar{l}_{\mathrm{r}_0}\omega_0^2 + 4\bar{l}_{\mathrm{r}_0}\omega^2$
13) compute λ_1, λ_2 and λ_3 using the initial condition
14) compute $\bar{r}$ using (13)
15) compute $\bar{p}_{\mathrm{g}}$ using (12)
16) compute p_{t} using (27)
17) compute $\hat{p}$ using (28)
18) $p_0 \leftarrow \hat{p}$
19) redo steps (10)–(13)
20) compute $r(t), \phi(t)$ using (11)
21) apply transformation from polar to Cartesian coordinates

Output: Approximate CoM trajectory in DS.

TABLE II
SYSTEM PARAMETERS AND INITIAL CONDITIONS USED IN SIMULATION

$k_0\,(\mathrm{kN/m})$	$\alpha^{\mathrm{w}}\,(\mathrm{degree})$	$\dot{x}_{\mathrm{v}}\,(\mathrm{m/s})$	$y_{\mathrm{v}}\,(\mathrm{m})$
$[10, 25]$	$[60^\circ, 80^\circ]$	$[0.5, 2]$	$[l_0 \sin\alpha, l_0]$

During the analysis, four dimensions are spanned: the initial horizontal velocity at VLO ($\dot{x}_{\mathrm{v}}$), the initial height at VLO (y_{v}), the legs' stiffness (k_0), and the touchdown angle (α^{w}). Table II shows the space of the varying parameters.

Without loss of generality, we set m = 80 kg, g = 9.81 m/s^2, and l_0 = 1 m in accordance with average human data, and limit the analysis to initial conditions with the vertical velocity at VLO ($\dot{y}_{\mathrm{v}}$) equal to zero. A trial is considered valid if 1) the system completes one walking step, and 2) it would be possible for the system to further touch down for the subsequent step. To satisfy the first condition, simulations in which the system leaves the ground (i.e., switching to an F phase), or when the CoM hits the ground or moves backward are excluded. Concerning the second condition, let $E_{\min}$ denote the minimum amount of the total mechanical energy at VLO required to make the subsequent touchdown

$$E_{\min} = mgl_0 \sin\alpha^{\mathrm{w}} + 1/2\, k_0 l_0^2 (1 - \sin\alpha^{\mathrm{w}})^2. \tag{29}$$

Then, the total mechanical energy as a function of the spanned variables $E(k_0, \alpha^{\mathrm{w}}, \dot{x}_{\mathrm{v}}, y_{\mathrm{v}})$ should satisfy the following

TABLE III
VRM APPROXIMATION ERROR

	mean	sd	max
e_{v}	1.0	1.4	18.0
$\mathcal{E}_{\mathrm{v}}$	1.7	2.6	32.7

property:

$$E(k_0, \alpha^{\mathrm{w}}, \dot{x}_{\mathrm{v}}, y_{\mathrm{v}}) \geq E_{\min}. \tag{30}$$

A total number of 5442 simulations (i.e., valid runs) satisfied these conditions. To quantify the prediction error in position, we use the following error measure expressed as a percentage:

$$e = 100\, \frac{||\xi_{\mathrm{true}} - \xi_{\mathrm{approx}}||_2}{||\xi_{\mathrm{true}}||_2} \tag{31}$$

where ξ is the CoM position in relationship to Cartesian coordinates (x, y). To measure the errors in the CoM velocity, to avoid division by zero due to normalization, we define another measure

$$\mathcal{E} = 100\, \frac{||\eta_{\mathrm{true}} - \eta_{\mathrm{approx}}||_2}{(||\eta_{\mathrm{true}}||_2)_{\max} - (||\eta_{\mathrm{true}}||_2)_{\min}} \tag{32}$$

where η is the CoM velocity. We evaluate the mean, standard deviation, and maximum value of these measures at the first return to the Poincaré section (i.e., at the next VLO), as reported in Table III. The position calculated using the approximate maps is sufficiently accurate and the velocity error remains within a small range.

Furthermore, a meaningful correlation between the fixed points of Poincaré map and the prediction accuracy of our approximate map can be observed. Define d_{v} to be a measure of the normalized distance between two subsequent returns at the Poincaré section[5]

$$d_{\mathrm{v}} = \left| \frac{y_{\mathrm{v}^+} - y_{\mathrm{v}^-}}{y_{\mathrm{v}^-}} \right| + \left| \frac{\dot{x}_{\mathrm{v}^+} - \dot{x}_{\mathrm{v}^-}}{\dot{x}_{\mathrm{v}^-}} \right|. \tag{33}$$

Fig. 5 depicts the prediction errors e_{v} and $\mathcal{E}_{\mathrm{v}}$ as functions of d_{v}. For each bin, the number of valid runs is shown to indicate which values are more likely to happen. A small value of d_{v} indicates that the system state at the Poincaré section is close to a fixed point. It can be seen in the figure that, in this situation, the approximation error is small too, meaning that the prediction is more accurate when the system state converges to the fixed points, which are of particular importance in most cases.

IV. APPLICATION TO GAIT CONTROL

In this section, we develop a class of controllers, relying on the presented analytical maps, that realize active gaits and gait transitions. In all the considered applications, the control system adjusts the legs' stiffness to inject the required energy necessary for achieving desired locomotion properties. To use the analytical maps derived in the previous section, we limit the variation of the leg compliance to discrete jumps, making the leg stiffness piecewise constant. Accordingly, every node in Fig. 2 that corresponds to stance phases has a constant stiffness that is reset when switching between the nodes. Once needed, the control system also modulates the touchdown angle to govern the interchange between kinetic and potential energy. Following this approach, which is sometimes (loosely) referred to as deadbeat control[6] [47], in the rest of this section, we synthesize controllers by realizing active walking, running, and its transitions. We then present a stability analysis and discuss the effect of approximations in this regard.

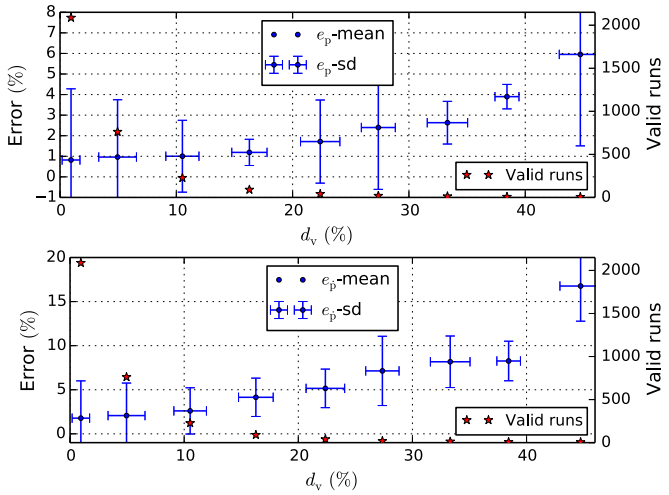

Fig. 5. Correlation between the system states at Poincaré section and the accuracy of the approximate VRM.

A. Active Running

The goal is to synthesize a controller that takes the given system state at a Poincaré section (z_{a^-}) to the desired state at the next return ($z^*_{\mathrm{a}^+}$). To do so, a controller 1) assigns different stiffnesses for $\mathrm{SS}^{\mathrm{r}}_{\mathrm{sc}}$ and $\mathrm{SS}^{\mathrm{r}}_{\mathrm{sd}}$, denoted by $k^{\mathrm{r}}_{\mathrm{sc}}$ and $k^{\mathrm{r}}_{\mathrm{sd}}$, respectively, and 2) adjusts the touchdown angle (α^{r}), which is used in the reset map upon the execution of the guard $\mathrm{G}^{\mathrm{r}}_{\mathrm{t}}$. The resulting controller is used once per step at apex where $\mathrm{G}^{\mathrm{r}}_{\mathrm{a}}$ fires. To complete the design of this controller, we further impose a constraint motivated by biological observations. From the experimental results reported in [48], it can be seen that during running the ratio of the maximum leg length change to the rest length is almost the same (≈ 0.1) across all participants and all running speeds, suggesting the following constraint on the spring length at the bottom state:

$$r_{\mathrm{b}} = \sigma \circ \mathcal{S}_{\mathrm{b}} = 0.9 l_0 \tag{34}$$

[5]Note that the conservation of the total energy dictates $(\dot{y}_{\mathrm{v}^+} - \dot{y}_{\mathrm{v}^-}) \to 0$, if $d_{\mathrm{v}} \to 0$.

[6]For a feasibility analysis of deadbeat control in the context of the SLIP hopper, see [46].

with σ being a projection operator. Now, we define the error equations as

$$\begin{aligned} z^*_{\mathrm{a}^+} - \mathcal{P}^{\mathrm{r}}(z_{\mathrm{a}^-}) &= \begin{bmatrix} e_1 & e_2 \end{bmatrix}^T \\ 0.9l_0 - r_{\mathrm{b}} &= e_3 \end{aligned} \tag{35}$$

where

$$\mathcal{P}^{\mathrm{r}}(\cdot) = \left({}^{\mathrm{a}^+}_{\mathrm{l}}\mathcal{P}^{\mathrm{r}} \circ {}^{\mathrm{l}}_{\mathrm{b}}\mathcal{P}^{\mathrm{r}} \circ {}^{\mathrm{b}}_{\mathrm{t}}\mathcal{P}^{\mathrm{r}} \circ {}^{\mathrm{t}}_{\mathrm{a}^-}\mathcal{P}^{\mathrm{r}} \right)(\cdot)$$

and $e_i \in \mathbb{R}$, $i \in \{1,2,3\}$ being the corresponding errors. The control inputs $u = \begin{bmatrix} k^{\mathrm{r}}_{\mathrm{sc}} & k^{\mathrm{r}}_{\mathrm{sd}} & \alpha^{\mathrm{r}} \end{bmatrix}^T$ are then the solution of the following optimization problem:

$$u = \arg\min \sum_i \rho_i e_i^2, \ i \in \{1,2,3\} \tag{36}$$

where $\rho_i \in \mathbb{R}$, $i \in \{1,2,3\}$, are weights of the corresponding criteria. They additionally normalize different terms of the cost function. In the simulation study reported later, we have set all the weights equal to one.

It is clear that the control inputs are bounded (i.e., the stiffness cannot take negative values, and the touchdown angle is between 0° and 90°). These requirements can either be formulated as constraints imposed to the optimization problem (36) or their undesired values can be penalized by some additional terms in the cost function. We use the latter option, as it gives more flexibility in the choice of the available optimization tools. Moreover, typical of nonlinear optimization problems, no guarantee for the existence or optimality of the solution can be given. However, our numerical investigations reveal a large domain of validity for the resulting solutions.

It has to be noted that a simplified approach for realizing active running can be found in the literature [40], [49], where $k^{\mathrm{r}}_{\mathrm{sc}}$ is manually chosen before executing the controller. Then, $k^{\mathrm{r}}_{\mathrm{sd}}$ is derived from the difference between the total energy of the system at current apex and the desired total energy at the subsequent apex. Next, the ARM is used to derive α^{r} numerically. Although this method is computationally simpler, preassigning $k^{\mathrm{r}}_{\mathrm{sc}}$ may lead to unfeasible values for $k^{\mathrm{r}}_{\mathrm{sd}}$, causing high discrete jumps in the stiffness profile. In contrast, our method gives the controller the flexibility to choose all the control inputs simultaneously. Moreover, we also impose the constraint (34) to the maximum leg retraction, which reinforces the similarity with biological evidence [48].

B. Active Walking

Producing active walking in the bipedal SLIP model is more challenging than active running due to the additional complexity imposed by the DS dynamics, and other constraints [50] on the system state. Studies investigating varying speed walking are mostly limited to intuitive approaches whereby the ankle push-off and torso pitch are exploited to regulate the walking speed [50]–[54]. The presence of feet (and thus ankles torque) is a crucial element in most of the existing controlled limit cycle walking models.

Since our bipedal SLIP is an abstract model without feet, in the following, we seek a simple method that enables the system to produce, to some degree, an active walking gait, based on the DS map introduced in this paper. Similarly to active running, we focus on an adjustable stiffness scheme. While several events can be chosen as the moment that either of the legs' stiffness is adjusted, we instantaneously adjust them at the virtual bottom defined in Section II-A. In fact, we have devised the walking hybrid automaton in Fig. 2 as the combination of four distinct modes such that it is suitable for the purpose of control design. In this sense, the virtual bottom event divides the DS phase of the bipedal SLIP into the virtual compression and decompression subphases denoted by $\mathrm{DS}^{\mathrm{w}}_{\mathrm{sc}}$ and $\mathrm{DS}^{\mathrm{w}}_{\mathrm{sd}}$, respectively.

The control problem here is defined as follows: given the VLO state at Poincaré section (z_{v^-}), the legs' stiffness and the touchdown angle are adjusted in such a way that the system converges to the desired state at the subsequent return ($z^*_{\mathrm{v}^+}$). Note that several constraints influence the reachability set of $z^*_{\mathrm{v}^+}$. In each walking cycle, irrespective of the phase being SS or DS, the legs' stiffness before the virtual bottom κ_1 is distinguished from that of after the virtual bottom κ_2. In other words,

$$k^{\mathrm{w}}_{\mathrm{av}} = k^{\mathrm{w}}_{\mathrm{sc}} = \kappa_1 \quad \text{and} \quad k^{\mathrm{w}}_{\mathrm{sd}} = k^{\mathrm{w}}_{\mathrm{bv}} = \kappa_2.$$

Following a similar process as for active running, we first define the error equation as:

$$z^*_{\mathrm{v}^+} - \mathcal{P}^{\mathrm{w}}(z_{\mathrm{v}^-}) = \begin{bmatrix} e_1 & e_2 & e_3 \end{bmatrix}^T \tag{37}$$

where

$$\mathcal{P}^{\mathrm{w}}(\cdot) = \left({}^{\mathrm{v}^+}_{\mathrm{l}}\mathcal{P}^{\mathrm{w}} \circ {}^{\mathrm{l}}_{\tilde{\mathrm{b}}}\mathcal{P}^{\mathrm{w}} \circ {}^{\tilde{\mathrm{b}}}_{\mathrm{t}}\mathcal{P}^{\mathrm{w}} \circ {}^{\mathrm{t}}_{\mathrm{v}^-}\mathcal{P}^{\mathrm{w}} \right)(\cdot).$$

Then, we solve (36) for the walking control inputs $u = \begin{bmatrix} \kappa_1 & \kappa_2 & \alpha^{\mathrm{w}} \end{bmatrix}^T$ with e_i, $i \in \{1,2,3\}$, as defined in (37).

The feasibility of the numerical solution of the resulting optimization may become restricted in some situations. Therefore, we also consider a modified control method that reduces the computational complexity motivated by Kalveram *et al.* [49], however, by constituting a relatively smaller domain of attraction. Given the system energy at VLO and the desired system energy at the next VLO, the difference between these two is to be compensated by the stiffness change at virtual bottom. This yields the following relation between κ_1 and κ_2:

$$\kappa_2 = \frac{\mu_4 + (\mu_3 - \mu_2)\kappa_1}{\mu_3 - \mu_1} \tag{38}$$

with

$$\begin{aligned} \mu_1 &= (l_0 - y^*_{\mathrm{v}^+})^2, \quad \mu_2 = (l_0 - y_{\mathrm{v}^-})^2 \\ \mu_3 &= (l_0 - l')^2 + (l_0 - l'')^2 \\ \mu_4 &= m\left((\dot{x}^*_{\mathrm{v}^+})^2 + (\dot{y}^*_{\mathrm{v}^+})^2 - (\dot{x}^2_{\mathrm{v}^-} + \dot{y}^2_{\mathrm{v}^-}) + 2g(y^*_{\mathrm{v}^+} - y_{\mathrm{v}^-})\right) \end{aligned}$$

where l' and l'' are the front and rear leg's length at virtual bottom, respectively. Now by presuming a reasonable value for κ_1 (e.g., $\kappa_1 \approx k_0$), the value of κ_2 can be immediately obtained using (38). Subsequently, the only remaining control parameter, $u = \alpha^{\mathrm{w}}$, is obtained by solving the optimization problem (36) with e_i, $i \in \{1,2,3\}$, as defined in (37). A quantitative demonstration of the method will be given in the simulations presented in the next sections.

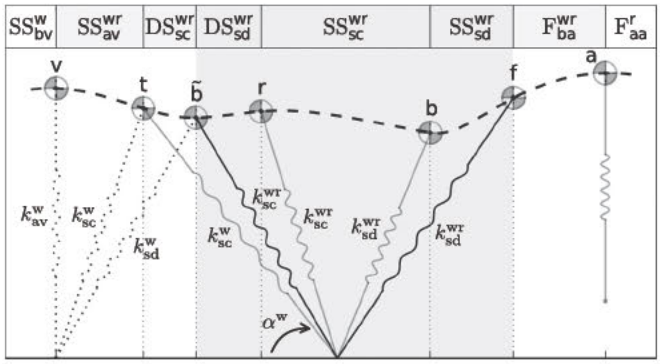

Fig. 6. Schematic of WRT. The controller is active in the shaded phases.

C. Walk–Run Transitions

Humans prefer to transition from walking to running at certain speeds. However, there is no unequivocal explanation as to why they change the gait [55]. It is also evidenced that the transition stride does not resemble either of the gaits [56], implying that this stride includes a sequence of transient dynamics that take the system state from a VRM to an ARM.

In the control literature, there are a few studies investigating walk–run transitions in the SLIP models. Hodgins [57] presented a simple leg lengthening approach, similar to Raibert's legs control (i.e., decoupled control of horizontal and vertical oscillations), that enables the walk–run transitions for a particular pair of walking and running speeds. Rummel *et al.* [16] identified an almost continuous morphing of gait patterns between walking and running in *passive* limit cycles at low and medium speeds. Martinez and Carbajal [17] detected a new intermediate gait pattern, *hopping*, that can connect a walking to a running limit cycle by exploiting two different touchdown angles in each stride. Neither of these papers deals with the varying compliance, something that is evidenced in the human motion [58]. Moreover, for the realization of walk–run transitions, switching to an intermediate gait (e.g., hopping) has not been identified in humans. Finally, humans and animals transition between walking and running during acceleration, the observation that we explore here on the SLIP model for the first time.

1) Walk-to-Run Transition: In this section, we synthesize a controller that takes the system state from walking to running. We take two biological observations into account: 1) the recorded trajectories of the humans' CoM during the WRT reported in [59]; and 2) the experiment carried out in [56] showing that the transition is not an abrupt event, and it is triggered in the transition stride and completed after an adjustment period. Motivated by these, we consider a WRT stride, as illustrated in Fig. 6, and we hypothesize that the WRT process is triggered at virtual bottom. This means that we have no control on α^{w}. An important assumption we make only for the control calculation is that the current DS phase is suddenly terminated at virtual bottom, and the system switches to a virtual SS phase. This phase ends with the liftoff event of the rear leg. In other words, in the design of the WRT controller, we ignore the influence of the rear leg after virtual bottom by considering a simplified model.

The process of transitioning can be described as follows. The system starts the transition stride at a VLO for which a particular condition (namely $\mathrm{G}^{\mathrm{wr}}_{\mathrm{v}}$) instructs the transition to running. The system walks in the same pace as the previous walking stride until the virtual bottom event ($\mathrm{G}^{\mathrm{wr}}_{\tilde{\mathrm{b}}}$). At this moment, the stiffness of the front leg is updated to a new value denoted by $k^{\mathrm{wr}}_{\mathrm{sc}}$, but the rear leg still uses the stiffness assigned by the walking controller $k^{\mathrm{w}}_{\mathrm{sd}}$. The next update in the stiffness occurs when the front leg is fully compressed corresponding to the bottom event, represented by guard $\mathrm{G}^{\mathrm{wr}}_{\mathrm{b}}$ in the hybrid automaton (see Fig. 2). The new stiffness, denoted by $k^{\mathrm{wr}}_{\mathrm{sd}}$, is then used until the liftoff event of the front leg $\mathrm{G}^{\mathrm{wr}}_{\mathrm{f}}$, leading the system to the $\mathrm{F}^{\mathrm{wr}}_{\mathrm{ba}}$ phase, which ends at apex.

On the implementation side, we construct the WRT map mapping z_{v} onto z_{a}

$$z_{\mathrm{a}} = \mathcal{P}^{\mathrm{wr}}(z_{\mathrm{v}}). \tag{39}$$

According to the hybrid automaton of the WRT in Fig. 2, $\mathcal{P}^{\mathrm{wr}}$ is a composition of the following submaps: the VLO to touchdown (${}^{\mathrm{t}}_{\mathrm{v}}\mathcal{P}^{\mathrm{wr}}$), the touchdown to virtual bottom (${}^{\tilde{\mathrm{b}}}_{\mathrm{t}}\mathcal{P}^{\mathrm{wr}}$), the virtual bottom to rear leg liftoff (${}^{\mathrm{r}}_{\tilde{\mathrm{b}}}\mathcal{P}^{\mathrm{wr}}$), the rear leg liftoff to bottom (${}^{\mathrm{b}}_{\mathrm{r}}\mathcal{P}^{\mathrm{wr}}$), the bottom to front leg liftoff (${}^{\mathrm{f}}_{\mathrm{b}}\mathcal{P}^{\mathrm{wr}}$), and the front leg liftoff to apex (${}^{\mathrm{a}}_{\mathrm{f}}\mathcal{P}^{\mathrm{wr}}$):

$$z_{\mathrm{a}} = ({}^{\mathrm{a}}_{\mathrm{f}}\mathcal{P}^{\mathrm{wr}} \circ {}^{\mathrm{f}}_{\mathrm{b}}\mathcal{P}^{\mathrm{wr}} \circ {}^{\mathrm{b}}_{\mathrm{r}}\mathcal{P}^{\mathrm{wr}} \circ {}^{\mathrm{r}}_{\tilde{\mathrm{b}}}\mathcal{P}^{\mathrm{wr}} \circ {}^{\tilde{\mathrm{b}}}_{\mathrm{t}}\mathcal{P}^{\mathrm{wr}} \circ {}^{\mathrm{t}}_{\mathrm{v}}\mathcal{P}^{\mathrm{wr}})(z_{\mathrm{v}}). \tag{40}$$

The analytical maps studied in Section III are used here to complete the derivation of the above relation. The control problem is to find the control inputs $u = \begin{bmatrix} k^{\mathrm{wr}}_{\mathrm{sc}} & k^{\mathrm{wr}}_{\mathrm{sd}} \end{bmatrix}^T$ that let the system converge to the desired system state at the subsequent apex z^*_{a}. As such, we first define the error equations as

$$z^*_{\mathrm{a}} - \mathcal{P}^{\mathrm{wr}}(z_{\mathrm{v}}) = \begin{bmatrix} e_1 & e_2 \end{bmatrix}^T. \tag{41}$$

Then, the control inputs u are the solution of an optimization problem that takes the same form as (36), where e_i, $i \in \{1, 2\}$, are determined by (41).

In the control calculation, the assumption that the DS phase suddenly ends at virtual bottom is made only to reinforce the following biological evidence observed for humans in [60]: "in the transition stride, the rear leg is walking and the front leg is running." Motivated by this, we keep the walking controller for the rear leg and introduce the WRT controller for the front leg. This means that the WRT controller uses a simplified model of the system dynamics (i.e., assuming no rear leg), while in the real simulation, the rear leg does push the system forward. As such, one must adapt the control system to compensate for this mismatch. Using physical insight and tuning in preliminary simulations, we have concluded that it is sufficient to adjust reference point z^*_{a}. Accordingly, in the simulation study presented in Section V, we use a relatively smaller value for $\dot{x}^*_{\mathrm{a}}$ and a larger value for y^*_{a} in comparison to the expected values.

Another note here is that $\mathrm{SS}^{\mathrm{wr}}_{\mathrm{sc}}$ may also contain a decompression phase prior to the compression phase. But since it has no consequence in the synthesis of the controller, to keep it simple, we do not further partition $\mathrm{SS}^{\mathrm{wr}}_{\mathrm{sc}}$ into two phases.

2) Run-To-Walk Transition: In the RWT, the running SLIP whose speed is decreasing transitions to the walking SLIP. We

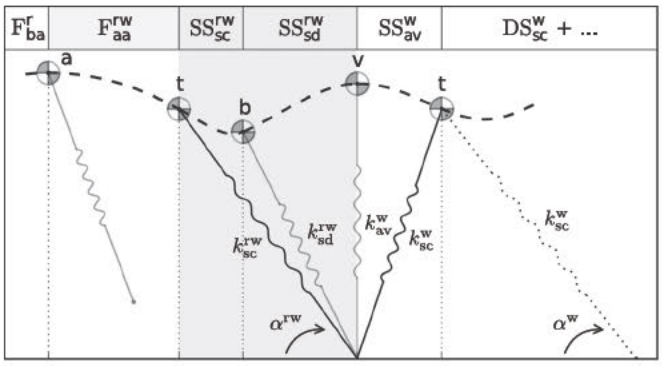

Fig. 7. Schematic of RWT. The controller is active in the shaded phases.

assume that the transition starts at the first apex whose horizontal velocity is less than the preferred RWT speed, and ends at the subsequent VLO. The RWT controller takes the running system state at apex (z_{a}) to the desired walking system state at VLO (z^{*}_{v}). Fig. 7 details the procedure we devised for the transition process schematically. Without loss of generality, we assume that the system trajectory, which has an oscillatory behavior, encompasses only one bottom event in the RWT process. Consequently, the sequence of the subphases that the system takes during the transition forms the RWT automaton in Fig. 2. The controller assigns a particular constant stiffness $k^{\mathrm{rw}}_{\mathrm{sc}}$ for $\mathrm{SS}^{\mathrm{rw}}_{\mathrm{sc}}$ and $k^{\mathrm{rw}}_{\mathrm{sd}}$ for $\mathrm{SS}^{\mathrm{rw}}_{\mathrm{sd}}$, and the RWT touchdown angle (α^{rw}) when the guard $\mathrm{G}^{\mathrm{rw}}_{\mathrm{t}}$ is fired. To formalize the problem, we first construct the RWT map that maps z_{a} to z_{v}

$$z_{\mathrm{v}} = \mathcal{P}^{\mathrm{rw}}(z_{\mathrm{a}}). \tag{42}$$

The map $\mathcal{P}^{\mathrm{rw}}$ is a composition of the following submaps: the apex to touchdown (${}^{\mathrm{t}}_{\mathrm{a}}\mathcal{P}^{\mathrm{rw}}$), the touchdown to bottom (${}^{\mathrm{b}}_{\mathrm{t}}\mathcal{P}^{\mathrm{rw}}$), and the bottom to VLO (${}^{\mathrm{v}}_{\mathrm{b}}\mathcal{P}^{\mathrm{rw}}$)

$$z_{\mathrm{v}} = \left({}^{\mathrm{v}}_{\mathrm{b}}\mathcal{P}^{\mathrm{rw}} \circ {}^{\mathrm{b}}_{\mathrm{t}}\mathcal{P}^{\mathrm{rw}} \circ {}^{\mathrm{t}}_{\mathrm{a}}\mathcal{P}^{\mathrm{rw}}\right)(z_{\mathrm{a}}). \tag{43}$$

For each of the associated submaps that belong to the three phases F, SS, and DS, we derived a mathematical expression in Section III. Similarly to the previous applications, we write the error equations

$$z^{*}_{\mathrm{v}} - \mathcal{P}^{\mathrm{rw}}(z_{\mathrm{a}}) = \begin{bmatrix} e_1 & e_2 & e_3 \end{bmatrix}^{T} \tag{44}$$

and then solve the optimization (36), with $e_i = i \in \{1, 2, 3\}$ as defined in (44). This yields the control inputs $u = \begin{bmatrix} k^{\mathrm{rw}}_{\mathrm{sc}} & k^{\mathrm{rw}}_{\mathrm{sd}} & \alpha^{\mathrm{rw}} \end{bmatrix}^{T}$ with which the system transitions from running to walking. A quantitative demonstration is presented in the simulation example reported in Section V-A.

D. Stability Analysis

For the SLIP model in running, any controller that modulates the touchdown angle and either the leg stiffness or the rest length grants the controllability of the system [30] with a reasonable basin of attraction [42]. Since the controller presented in Section IV-A meets this requirement, we therefore omit the stability analysis of the running gait. On the other hand, the stability and robustness of the controlled SLIP walking introduced in Section IV-B have not been studied. In particular, since the controller uses the novel approximate return map, the effect of approximation errors on the robustness of the resulting controlled system needs to be carefully analyzed.

The stability of a fixed point of the VRM ($\mathcal{P}^{\mathrm{w}}$) is determined by studying the effect of a small perturbation in its neighborhood. This is typically approximated by using the corresponding Taylor expansion. If the eigenvalues of the associated Jacobian are inside the unit circle, then the intended fixed point is stable, thereby an associated basin of attraction exists. The relative location of the fixed point inside its basin of attraction and the size of the basin indicate how robust the controlled system is.

Obtaining the exact basin of attraction for the SLIP model is not always straightforward. An intuitive *steps-to-fall* method for obtaining an approximation of the domain has been used in [15] and [19]. Through a numerical search in the neighborhood of the equilibrium point, all the initial conditions leading to a predefined minimum number of successive steps with the Poincaré states converging to the equilibrium are collected to form an approximation of the basin of attraction. Following this approach for the passive SLIP model, *self*-stable fixed points have already been identified [15], [17], [19]. Vejdani *et al.* [61] obtained a larger domain of attraction with provably the fastest convergence rate, by modulating the touchdown angle. This study is based on the fact that, in the context of deadbeat control, more than one walking step is required to grant control authority on the SLIP model [46]. The authors derived the domain of attraction of the two-step deadbeat stabilized gaits via backward-in-time integration of the system dynamics.

The exact pinpointing of the desired equilibrium is a strict and mostly unnecessary requirement imposed to the control system, which can readily be violated in many situations. In practice, it is sufficient if the controller takes the Poincaré state to the self-stable region of the equilibrium. Then, by definition, the state will remain in this small neighborhood of the equilibrium and will asymptotically converge to it in a finite number of steps. Therefore, even for the one-step walking control, a meaningful domain of attraction can be obtained, if the exact pinpointing constraint is relaxed. This also enables the analysis of the effect of approximation on the control performance, while the deadbeat control of the system is generally infeasible when the dynamics are represented by approximate solutions.

A walking trajectory of the passive SLIP model can be fully determined by the Poincaré state z_{v}, the dimensionless stiffness ($\tilde{k}_0 = k_0 l_0/(mg)$), the dimensionless energy ($\tilde{E} = E/(l_0 mg)$), and the touchdown angle (α^{w}) [15].[7] To express the Poincaré state, one can use the triple $\begin{bmatrix} y_{\mathrm{v}} & \phi_{\mathrm{v}} & E \end{bmatrix}^{T}$ instead of the already defined $\begin{bmatrix} \dot{x}_{\mathrm{v}} & y_{\mathrm{v}} & \dot{y}_{\mathrm{v}} \end{bmatrix}^{T}$, as it is more convenient for the stability analysis, where ϕ_{v} denotes the velocity angle at the Poincaré section. The velocity magnitude v_{v} can be calculated from the system energy E, since the system is passive. Given an appropriate k_0, there exists a one-to-one relationship between E and α^{w} for a certain domain of E following which

[7] Without loss of generality, we shall use the dimensional counterparts by assuming the following numerical values: $m = 80\,\mathrm{kg}, l_0 = 1\,\mathrm{m}, g = 9.81\,\mathrm{m/s^2}, k_0 = 16.5\,\mathrm{kN/m}$.

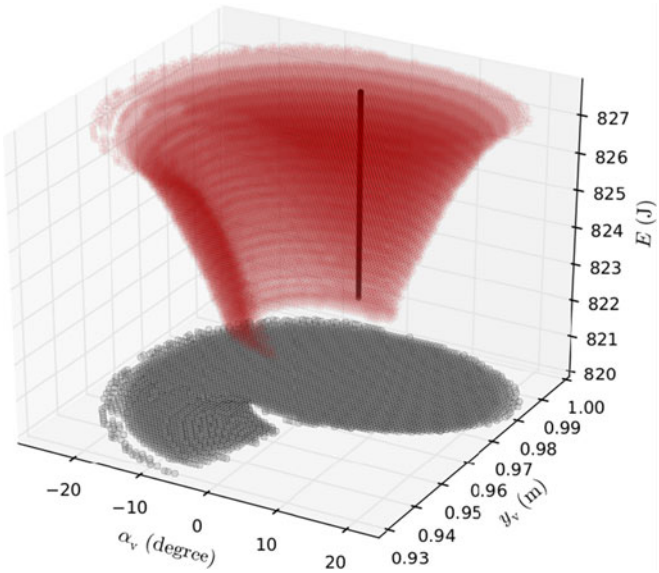

Fig. 8. Self-stable basin of attraction of the intended set of equilibria depicted by the black line.

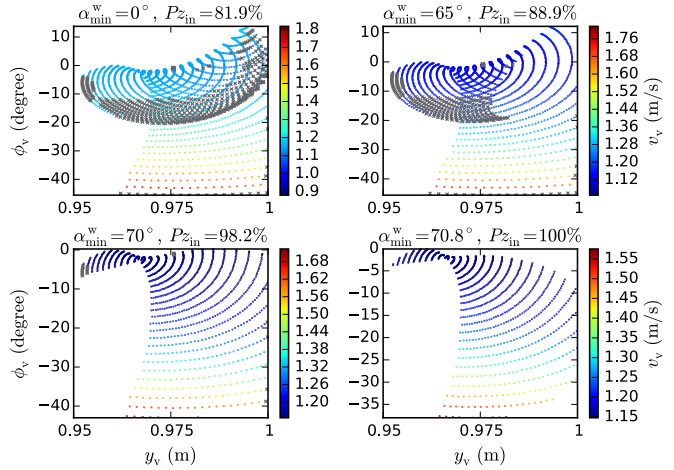

Fig. 9. Effect of approximation on the domain of attraction for the proposed walking controller. The gray crosses indicate where the controller fails to stabilize the equilibrium.

an equilibrium point is stable. We identified the self-stable basin of attraction of the equilibrium $\bar{z}_v = [0.9818\,\mathrm{m}\ \ 0\ \ E]^T$ with $E \in [822.06\,\mathrm{J}\ \ 827.62\,\mathrm{J}]$, by following the steps-to-fall approach,[8] as shown in Fig. 8.

We shall now identify the basin of attraction for the one-step deadbeat stabilization of the same equilibrium in the active SLIP walking, with the control policy following the modified method presented in Section IV-B. In doing so, we integrate the "exact" return map backward-in-time starting from the initial condition that coincides with the equilibrium ($\bar{z}_v = [0.9818\,\mathrm{m}\ \ 0\ \ 826\,\mathrm{J}]^T$), while spanning the control parameters $\kappa_2 \in [0.5k_0\ \ 1.5k_0]$ and $\alpha^w \in [0^\circ\ \ 90^\circ]$. We repeat the same computation by using the introduced approximate map and construct a lookup table for the control inputs $u = [\kappa_2\ \ \alpha^w]^T$ accordingly. Now for the initial states belonging to the domain of attraction, we shall check to what extent the resulting state is inside the self-stable domain, if the control parameters of the approximate solution are used. Let Pz_{in} be the corresponding relative percentage, calculated accordingly.

Fig. 9 illustrates the obtained results. As can be seen, by increasing the lower bound of the touchdown angle (α^w_{min}), which increases the validity domain of our approximations according to assumption (16), one can obtain larger Pz_{in} so that for a certain lower bound ($\alpha^w_{min} = 70.8^\circ$) Pz_{in} reaches 100%. This means that the walking controller based on our approximate solution succeeds in stabilizing all the Poincaré states belonging to the domain of attraction, provided that the touchdown angle is bounded from below to that particular value. Although the approximate nature of the controller precludes the possibility of exact pinpointing, the state is brought to the self-stable domain such that y_v and ϕ_v converge to the equilibrium and v_v converges to a constant value in the domain $[1.11\,\mathrm{m/s}\ \ 1.17\,\mathrm{m/s}\ ]$. A similar numerical analysis can be performed for other equilibrium points representing human-like walking.

[8]The minimum number of steps is set to 50. Also, note that the given specific value of vertical position at VLO, i.e., $y_v = 0.9818\,\mathrm{m}$, was selected based on legacy.

V. Simulation and Results

In this section, we demonstrate the utility of the proposed framework in simulation. In a first example, we consider a locomotion scenario that humans usually follow to speed up and slow down. A second example is provided to explore one possibility of using the obtained controlled SLIP model as target dynamics for the control of a multibody walking robot.

The simulations were carried out in Python 2.7, and the results were plotted in Matplotlib 1.3. All the optimizations and implicit equations involved in the control calculations, including those that govern the transition guards, were solved using the `scipy.optimize.root` function.

A. Example I: Human-Like Motions on the Controlled Spring-Loaded Inverted Pendulum

According to Fig. 10, the SLIP model starts walking with an initial condition close to (but not necessarily belong to) a passive limit cycle with the average (per-stride) locomotion speed of $\dot{\bar{x}} = 1.17\,\mathrm{m/s}$ up to the time $t_{wr} = 0.8\,\mathrm{s}$. The modified walking controller proposed in Section IV-B guides the system in this phase. At the first step after t_{wr}, the WRT controller is activated. The control parameters k^{wr}_{sc} and k^{wr}_{sd} that lead to the WRT, as proposed in Section IV-C1, are computed, and the transition takes place according to the hybrid automaton introduced in Fig. 2. The robot is then commanded to run with the average acceleration of $a = 1.05\,\mathrm{m/s^2}$, while keeping the same height as that of the walking gait ($y^*_a = y^*_v = 0.98\,\mathrm{m}$). The robot stops accelerating at a certain instant and keeps a constant locomotion speed of $\dot{\bar{x}} = 5\,\mathrm{m/s}$ for 1.5 s. Next, a decelerated run with the same rate is considered. All the running phases are controlled following the method described in Section IV-A. At the first apex for which the horizontal velocity is less than the preferred

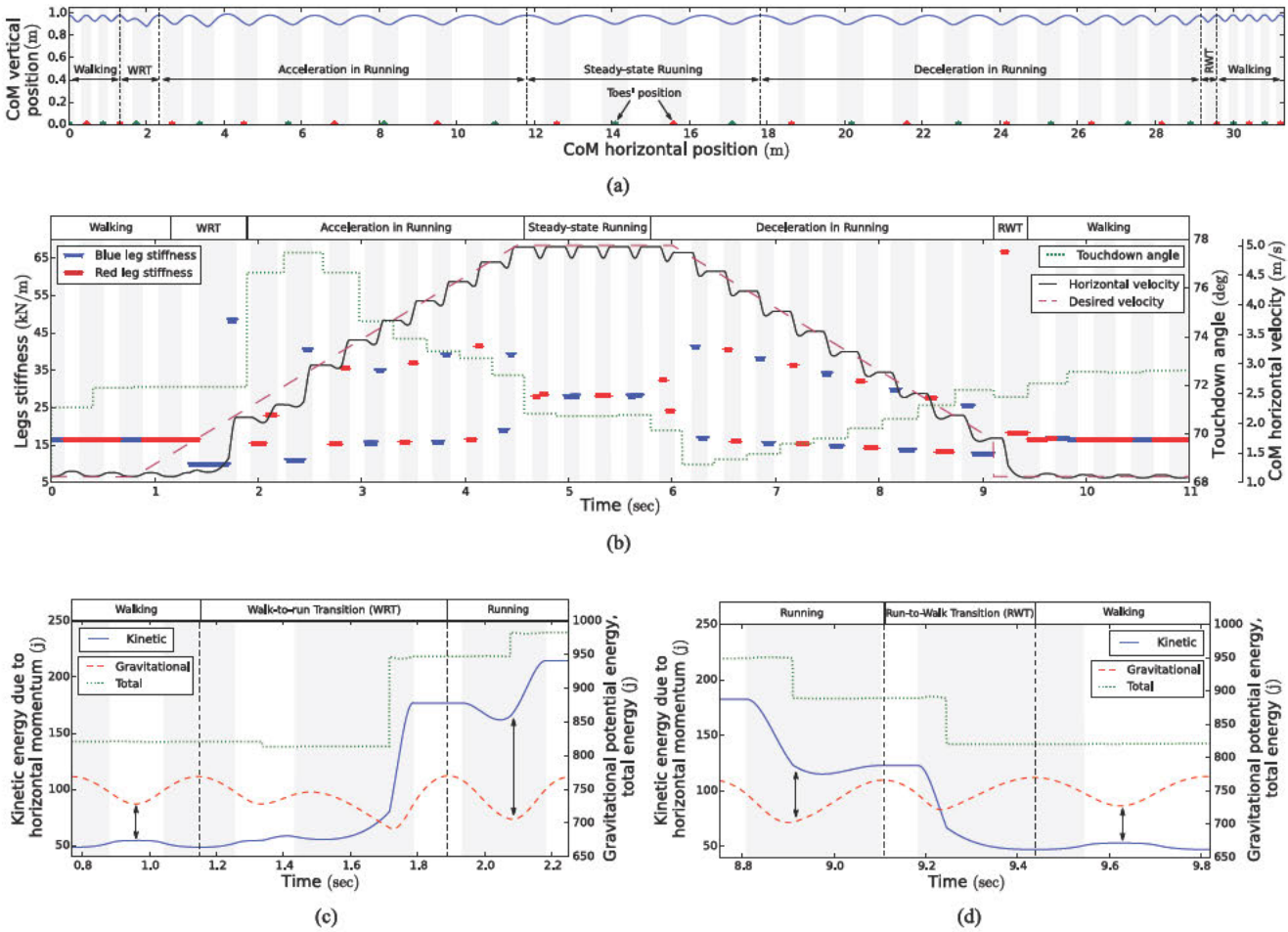

Fig. 10. Simulation of a bipedal SLIP model. The system starts in walking, switches to running with first increasing and then decreasing speed and finally transitions back to walking. The corresponding SS phases are shaded in each panel. (a) CoM trajectory and toes' position (footholds). (b) Control inputs together with the horizontal velocity of CoM. The dashed line is the set from which the desired velocity at apex/VLO is chosen. (c) Energetics of the system during WRT. The gravitational potential energy and the kinetic energy due to horizontal momentum are out-of-phase in walking (before the transition) and in-phase in running (after the transition). (d) Energetics of the system during RWT. The gravitational potential energy and the kinetic energy due to horizontal momentum are in-phase in running (before the transition) and out-of-phase in walking (after the transition).

RWT speed (2 m/s), the RWT controller, proposed in Section IV-C2, is invoked and the control parameters $k_{\mathrm{sc}}^{\mathrm{rw}}$, $k_{\mathrm{sd}}^{\mathrm{rw}}$, and α^{rw} are calculated accordingly. Consequently, the robot transitions back to the initial walking limit cycle.

Results and discussion: The CoM trajectory together with the toes' positions are plotted in Fig. 10(a). Fig. 10(b) shows the control parameters, namely the legs' stiffness and the touchdown angle. In addition, the horizontal CoM velocity and the set, from which the desired horizontal velocities at apex/VLO are chosen, are depicted. Finally, Fig. 10(c) and (d) depicts the energetics of the system around the transition gaits, where the gravitational potential energy, the kinetic energy due to horizontal momentum, and the total system energy are plotted. In each plot, the corresponding SS phases are shaded and the gait markers are used. The detailed view for the WRT and RWT were already given in Figs. 6 and 7. Also, Table IV reports summary information on the variables used in the simulation along with the corresponding results.

As can be seen in the results, active walking and running gaits together with their transitions are realized effectively in simulation. In the following, we explore some of the important features that can be identified from the results.

Relevance and feasibility analysis: To evaluate the feasibility of the results, we compare the leg stiffness obtained in our simulation to experimental observations. Even though the calculated stiffness in our work is entirely derived using (36) without *a priori* knowledge, there is a good match to the experimental values reported in [48, Fig. 1] for the human. As an example, the mean value of the measured leg stiffness of several participants for the speeds of 4.5 and 5.5 m/s roughly equal to 30.8 and 31.4 kN/m, respectively. The computed leg stiffness in our method for the speed of 5.0 m/s is 28.2 kN/m [see Fig. 10(b)], which seems relevant when compared to the experimental results. This match holds also for all other speeds reported, partly owing to the constraint (34) we have used in Section IV-A. Moreover, the trajectory of the CoM during the WRT, depicted in Fig. 10(a), resembles that observed for a human in [59] qualitatively.

As depicted in Fig. 10(b), in the accelerated run, the controller commands a smaller stiffness for the compression compared to

TABLE IV
SYSTEM AND CONTROL PARAMETERS

System parameters:			
Body mass	m	80	kg
Gravity acceleration	g	9.81	$\mathrm{m/s^2}$
Leg rest length	l_0	1	m
Initial condition:			
$\dot{x}$ at starting VLO	$\dot{x}_{\mathrm{v}}$	1.1	m/s
y at starting VLO	y_{v}	0.98	m
$\dot{y}$ at starting VLO	$\dot{y}_{\mathrm{v}}$	0	m/s
Initial control parameters:			
Leg stiffness	k_0	16.5	kN/m
Touchdown angle	α^{w}	70	degree
WRT (See Fig. 6)			
$z_{\mathrm{a}}^* = [\,\dot{x}_{\mathrm{a}}^*\ \ y_{\mathrm{a}}^*\,]^T = [\,0.6\ \ 1.6\,]^T$			
$z_{\mathrm{v}} = [\,\dot{x}_{\mathrm{v}}\ \ y_{\mathrm{v}}\ \ \dot{y}_{\mathrm{v}}\,]^T = [\,1.101\ \ 0.9797\ \ -0.0442\,]^T$			
$[\,\alpha^{\mathrm{w}}\ \ k_{\mathrm{sc}}^{\mathrm{w}}\ \ k_{\mathrm{sd}}^{\mathrm{w}}\,]^T\vert_{\text{WRT-stride}} = [\,71.94\ \ 16.50\ \ 16.50\,]^T$			
$[\,k_{\mathrm{sc}}^{\mathrm{wr}}\ \ k_{\mathrm{sd}}^{\mathrm{wr}}\,]^T = [\,9.860\ \ 48.51\,]^T$			
RWT (See Fig. 7)			
$z_{\mathrm{v}}^* = [\,\dot{x}_{\mathrm{v}}^*\ \ y_{\mathrm{v}}^*\ \ \dot{y}_{\mathrm{v}}^*\,]^T = [\,1.1\ \ 0.98\ \ 0\,]^T$			
$z_{\mathrm{a}} = [\,\dot{x}_{\mathrm{a}}\ \ y_{\mathrm{a}}\,]^T = [\,1.754\ \ 0.9766\,]^T$			
$[\,\alpha^{\mathrm{rw}}\ \ k_{\mathrm{sc}}^{\mathrm{rw}}\ \ k_{\mathrm{sd}}^{\mathrm{rw}}\,]^T = [\,71.53\ \ 66.97\ \ 18.35\,]^T$			

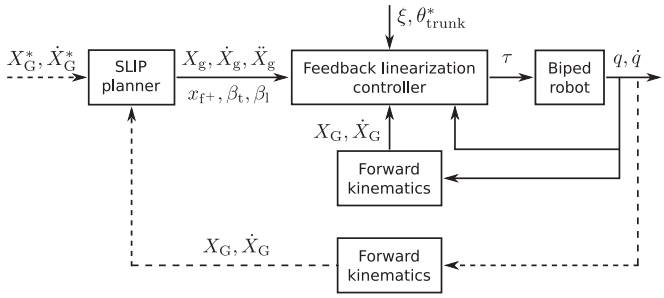

Fig. 11. Block diagram of the overall control system developed to reproduce SLIP dynamics in a multibody robot. The superscript "$*$" denotes the reference value.

the decompression phase, which increases the system energy level. Combined with the influence of the touchdown angle, this shortens the decelerating part and prolongs the accelerating part in each stance phase, which can be seen in the same figure. Consequently, the locomotion speed and the step length increase. In contrast, for the decelerated run, the stiffness in the compression phase takes a larger value, resulting in smaller steps with reduced speeds.

Energy-based analysis: There is a common way of defining the walking and running gaits in biomechanics, which is related to dynamical characteristics: the involved fluctuations in kinetic energy due to forward momentum and gravitational potential energy that are out-of-phase in walking and in-phase in running [59]. This can be seen in Fig. 10(c) and (d) for the controlled system we developed in this study. Of particular interest are the transition periods in which the shape of the mentioned fluctuations before and after the transition are different in result of the changes in the legs' compliance and touchdown angle.

Effect of approximation: The magnitude of approximation errors and its effect on the stability of the proposed controlled system were studied in Sections III-D and IV-D, respectively. As an example here, while the RWT controller is supposed to take the system states to $z_{\mathrm{v}}^* = [\,\dot{x}_{\mathrm{v}}^*\ \ y_{\mathrm{v}}^*\ \ \dot{y}_{\mathrm{v}}^*\,]^T = [\,1.1\ \ 0.98\ \ 0\,]^T$, due to the mentioned errors, the system converges to $z_{\mathrm{v}} = [\,1.085\ \ 0.9807\ \ -0.018\,]^T$ instead. If the controller was turned OFF in the subsequent limit cycle walking, the system would lose stability, although it could walk for a number of steps. The active walking system, however, compensates for the mentioned error so that the system can walk for an infinite number of steps.

B. Example II: Spring-Loaded Inverted Pendulum-Like Motions in Multibody Robot Walking

We now present an example of application to bipedal walking in which the controlled SLIP model is used as a planner for the control of a multibody robot model. The problem of controlling walking robots based on the bipedal SLIP model has been studied by taking a feedback linearization-based approach [23] and optimization-based approaches [62], [63]. The method we follow in this section is inspired by Garofalo *et al.* [23]; however, aimed at performing a maximal mapping between the real robot and the SLIP model, we extend the previous results. Therefore, we shall focus here on the specific contribution made, and refer readers to consult [23] for the description of the model and the detailed derivations of the equations of motion, contact model, and control policy.

The considered robot model is the standard planar 5-DoF biped robot with point feet, as depicted in Fig. 12. To have an appropriate coordinate variable that can be shared between the robot and its SLIP planner, we similarly use the relative angle β defined between the horizontal and the line connecting the rear stance foot to the CoM (see Fig. 12). The trajectories planned by the SLIP model (namely the CoM position, velocity, and acceleration) are parameterized as functions of β. Further, the generated swing foot trajectories[9] using the virtual constraint ξ, as defined in [23, eq. (13)], are also expressed as functions of β.

The structure of the overall control system is depicted in Fig. 11. Continuous and event-driven signals are depicted in the solid and dashed lines, respectively. The SLIP planner, which uses the modified walking controller proposed in Section IV-B, is invoked once per step at VLO. It provides the controller with the CoM trajectories $X_{\mathrm{g}}, \dot{X}_{\mathrm{g}}, \ddot{X}_{\mathrm{g}}$, the next touchdown foot position x_{f^+}, and the relative angle in the next touchdown and liftoff events $\beta_{\mathrm{t}}, \beta_{\mathrm{l}}$. The latter two are used in the generation of the swing foot trajectories. The controller unit performs the following tasks:

1) the SLIP trajectory tracking by the robot's CoM;
2) the swing foot reference trajectory tracking by satisfying the virtual constraint ξ;
3) the trunk stabilization at the desired posture.

Different from the approach taken in [23], we instruct the robot's CoM to track the SLIP trajectories not only in the acceleration level, but also in the position and velocity levels, leading

[9]For the swing foot reference trajectory, we use circular arcs for the sake of demonstration. More sophisticated trajectories are available in the literature, whose implementation is, however, beyond the scope of this paper.

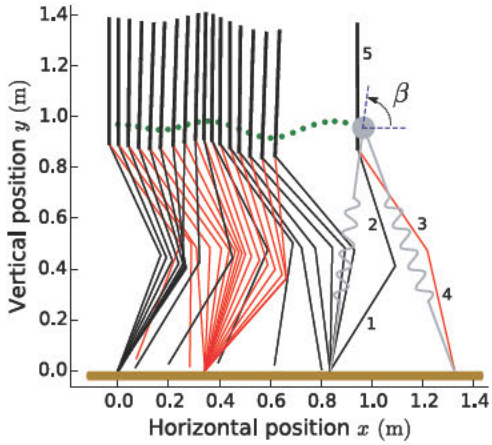

Fig. 12. Stick diagram of the walking gait produced by the controller that uses the SLIP template information.

to a complete coordination between the two systems. This is feasible owing to the analytical simplicity of the derived approximations, based on which the proposed walking controller is formulated. As such, the reference terms in the control policy (see [23, eq. (20)]) need to be adapted. This is done by revising [23, eq. (21)] to the following:

$$\ddot{X}_{\text{task}} = \begin{bmatrix} \ddot{X}_{\text{g}} + k_{P_{\text{g}}}(X_{\text{g}} - X_{\text{G}}) + k_{D_{\text{g}}}(\dot{X}_{\text{g}} - \dot{X}_{\text{G}}) \\ -K_{P_\xi}\xi - K_{D_\xi}\dot{\xi} \\ \ddot{\theta}^{*}_{\text{trunk}} + k_{P_{\text{trunk}}}\tilde{\theta}_{\text{trunk}} + k_{D_{\text{trunk}}}\dot{\tilde{\theta}}_{\text{trunk}} \end{bmatrix} \tag{45}$$

where $X_{\text{g}} = [x \;\; y]^T$ and $X_{\text{G}} = [x_{\text{G}} \;\; y_{\text{G}}]^T$ are the vector of CoM positions for the SLIP and robot model, respectively, $k_{P_{\text{g}}}$ and $k_{D_{\text{g}}}$ are proportional and derivative gains associated with the position and velocity errors, and the rest as defined in [23].

Results and discussion: We implement the presented control strategy on the 5-DoF robot model in simulation. For the sake of comparison, we choose the same numerical values for the simulation parameters as in [23]. The initial condition ($z_0 = [0.9695\,\text{m} \;\; 1.9^\circ \;\; 821.55\,\text{J}]^T$) is chosen from the obtained basin of attraction in Fig. 9, thereby the stabilization of the equilibrium point in the SLIP planner is guaranteed. Based on the simulation results, we show that the real robot also stabilizes *the same* equilibrium point.

Fig. 12 shows the stick diagram of the robot walking produced by the presented control strategy. The green dots are the positions of the robot's CoM. One can see that they perfectly coincide with the SLIP positions as compared in Fig. 13(a). Note that the method proposed in [23] fails to stabilize the same equilibrium point. This full control authority is useful especially for the transient behaviors, such as gait transitions, for which the computational burden of planning can partly be passed to the SLIP control, as investigated in this paper.

As shown in Fig. 11, the rear leg of the robot lifts off at the same configuration (namely, the same β_1) as that of SLIP. Aimed at reducing the required control inputs, we also explore an independent condition in which the leg lifts off at a predefined configuration. The corresponding control inputs (namely, joint

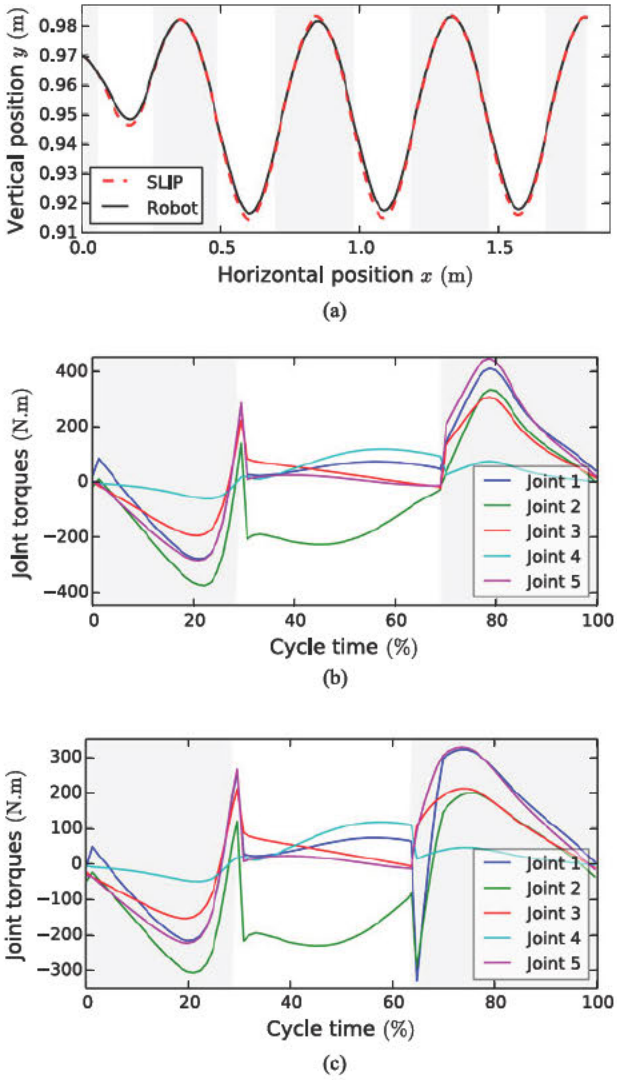

Fig. 13. Simulation results of embedding SLIP dynamics into the multibody robot. The corresponding SS phases are shaded in each panel. (a) CoM trajectories. (b) Joint inputs with the same liftoff states as those of SLIP. (c) Joint inputs with predefined liftoff states.

torques) for a single step of walking for both cases are plotted in Fig. 13(b) and (c). It is clear that although the torques' amplitudes in the latter case are reduced, the associated profiles at the liftoff transition are smoother when the SLIP information is used.

It seems that even the reduced torques are still rather large. Notice that the simulation model is instructed to walk at around normal pedestrian speeds, which is a relatively challenging task for an 80 kg humanoid. Nevertheless, we suspect that optimizing the distribution of physical parameters and the swing leg dynamics can additionally reduce the control inputs, which is an interesting topic for future research.

Remark on stability: Since the biped robot is instructed to exactly reproduce the controlled SLIP dynamics, its stability follows the same properties. However, due to external disturbances (such as the effect of touchdown impact) and uncertainties, the robot can encounter robustness issues. Nevertheless, the

robustness properties of the feedback linearization-based controllers have extensively been studied, and we therefore invite interested readers to consult the relevant literature.

VI. Conclusion

We have introduced a unified framework for walking, running, and walk–run transitions on the bipedal SLIP. We have shown that by assuming a piecewise constant profile for the stiffness of the bipedal SLIP, together with the modulation of the touchdown angle, one can synthesize controllers that create varying speed gaits and their transitions. Choosing different stiffness for the spring compression and decompression phases grants the required changes needed in the system's total energy level. In addition, the leg touchdown angle can modulate the interchange between kinetic and potential energy that is necessary for locomotion speed regulation.

The control signal calculations substantially rely on the approximate analytical maps of the otherwise nonintegrable stance dynamics. Although a number of approximations have been proposed for the SS dynamics, the DS analytical solutions remained unsolved. In this paper, we also proposed a novel approximate solution to this problem, by introducing an auxiliary system (AT-SLIP) whose CoM trajectories roughly coincide with the original bipedal SLIP trajectories during DS. The prediction error of the solution was analyzed via numerical simulations covering a large range of initial conditions and system parameters. The approximate solution given in Algorithm 1 was used to generate an active stable walking gait in situations in which the passive SLIP fails.

The stability/robustness of the resulting controlled system was analyzed numerically. The negative effect of approximations on the robustness of the controller was compensated by subjecting the controllable touchdown angle to a certain lower bound. In other words, the proposed approximations are more effective for the human-like walking gaits (i.e., for larger touchdown angles). For the deadbeat-form controllers, we also expanded the existing results on the stability analysis by leveraging on the self-stability properties of the SLIP model.

Concerning the control calculations, the presented method utilizing the approximate analytical maps is substantially faster than the methods based on numerical integrations. Our preliminary investigations revealed that it can be run online on a real (higher-dimensional) robot to generate target (desired) dynamics that can be treated as guidelines for the real system, as demonstrated in simulation. We are currently investigating control of a dynamic quadrupedal robot by embedding the proposed controlled SLIP in its legs.

Appendix
Details on Derivations Presented in Sections II and III

A. Section II—Equations (2) and (3)

Denoting by θ_i the angle between the ith leg and the horizontal plane, and by l_i the ith leg length (see Fig. 1), the following expressions complete the corresponding representations:

$$\theta_1(x,y) = \arctan\frac{y}{x-c_1}, \quad \theta_2(x,y) = \arctan\frac{y}{x-c_2}$$

$$l_1(x,y) = \sqrt{(x-c_1)^2+y^2},\ l_2(x,y) = \sqrt{(x-c_2)^2+y^2}$$

$$T_{\mathrm{SS}_i}(x,y) = \begin{bmatrix}\cos\theta_i(x,y)\\ \sin\theta_i(x,y)\end{bmatrix}, \quad i\in\{1,2\}$$

$$T_{\mathrm{DS}}(x,y) = \begin{bmatrix}\cos\theta_1(x,y) & \cos\theta_2(x,y)\\ \sin\theta_1(x,y) & \sin\theta_2(x,y)\end{bmatrix}$$

$$F_{\mathrm{l}_i}(x,y) = k_0(l_0 - l_i(x,y)), \quad \text{for } l_i \le l_0, \quad i\in\{1,2\}.$$

B. Section III-C1—Definition of Polar Coordinates (r,ϕ)

Polar coordinates represented by the pair (r,ϕ) are defined with the following relationship to Cartesian coordinates (see Fig. 4):

$$r(x,y) = \sqrt{(x-c/2)^2+y^2}$$
$$\phi(x,y) = \arctan\frac{y}{x-c/2}$$

where $\phi(x,y)$ is measured from the horizontal, and the coordinates' origin is at $x=c/2$, with c being the step length.

C. Section III-C1—Equation (15)

Referring to Fig. 4, the following expressions are given:

$$T_{\mathrm{AT}}(x,y) = \begin{bmatrix}\cos\phi(x,y) & -\sin\phi(x,y)\\ \sin\phi(x,y) & \cos\phi(x,y)\end{bmatrix}$$

$$F_{\mathrm{r}}(x,y) = k_{\mathrm{r}}\left(l_{\mathrm{r}_0} - r(x,y)\right)$$

$$F_{\mathrm{t}}(x,y) = k_{\mathrm{t}}\left(\frac{\phi_0 - \phi(x,y)}{r(x,y)}\right).$$

D. Section III-C1—Equations (22)

The following matrices are required to solve (22):

$$A = T_{\mathrm{AT}}(x,y)\begin{bmatrix}y_{\mathrm{eq}} - r(x,y) & 0\\ 0 & \dfrac{\phi_0-\phi(x,y)}{r(x,y)}\end{bmatrix}$$

$$B = T_{\mathrm{DS}}(x,y)\begin{bmatrix}F_{\mathrm{l}_1}(x,y)\\ F_{\mathrm{l}_2}(x,y)\end{bmatrix} - T_{\mathrm{AT}}\begin{bmatrix}mg\\ 0\end{bmatrix}.$$

References

[1] J. Diamond, "Why animals run on legs, not on wheels," *Discover*, vol. 4, no. 9, pp. 64–67, 1983.

[2] R. J. Full and D. E. Koditschek, "Templates and anchors: Neuromechanical hypotheses of legged locomotion on land," *J. Exp. Biol.*, vol. 202, no. 23, pp. 3325–3332, 1999.

[3] R. Alexander, "Mechanics of bipedal locomotion," *Perspectives Exp. Biol.*, vol. 1, pp. 493–504, 1976.

[4] R. Blickhan, "The spring-mass model for running and hopping," *J. Biomechan.*, vol. 22, no. 11, pp. 1217–1227, 1989.

[5] G. Cavagna, F. Saibene, and R. Margaria, "Mechanical work in running," *J. Appl. Physiol.*, vol. 19, no. 2, pp. 249–256, 1964.

[6] R. Alexander and A. Jayes, "Vertical movements in walking and running," *J. Zool.*, vol. 185, no. 1, pp. 27–40, 1978.

[7] T. A. McMahon and G. C. Cheng, "The mechanics of running: How does stiffness couple with speed?" *J. Biomechanics*, vol. 23, pp. 65–78, 1990.

[8] M. H. Raibert, *Legged Robots That Balance*, vol. 3. Cambridge, MA, USA: MIT Press, 1986.

[9] P. Gregorio, M. Ahmadi, and M. Buehler, "Design, control, and energetics of an electrically actuated legged robot," *IEEE Trans. Syst., Man, Cybern., B, Cybern.*, vol. 27, no. 4, pp. 626–634, Aug. 1997.

[10] M. Ahmadi and M. Buehler, "Controlled passive dynamic running experiments with the ARL-monopod II," *IEEE Trans. Robot.*, vol. 22, no. 5, pp. 974–986, Oct. 2006.

[11] B. Brown and G. Zeglin, "The bow leg hopping robot," in *Proc. IEEE Int. Conf. Robot. Autom.*, 1998, vol. 1, pp. 781–786.

[12] U. Saranli, M. Buehler, and D. E. Koditschek, "RHex: A simple and highly mobile hexapod robot," *Int. J. Robot. Res.*, vol. 20, no. 7, pp. 616–631, 2001.

[13] R. Playter, M. Buehler, and M. Raibert, "BigDog," *Proc. SPIE , Unmanned Syst. Technol. VIII*, vol. 6230, 2006, Art. no. 62 302O.

[14] J. A. Grimes and J. W. Hurst, "The design of ATRIAS 1.0 a unique monoped, hopping robot," in *Proc. Int. Conf. Climbing Walking Robots Support Technol. Mobile Mach.*, 2012, pp. 548–554.

[15] H. Geyer, A. Seyfarth, and R. Blickhan, "Compliant leg behaviour explains basic dynamics of walking and running," *Proc. Roy. Soc. B, Biol. Sci.*, vol. 273, no. 1603, pp. 2861–2867, 2006.

[16] J. Rummel, Y. Blum, and A. Seyfarth, "From walking to running," in *Proc. Autonome Mobile Systeme*, 2009, pp. 89–96.

[17] H. R. Martinez and J. P. Carbajal, "From walking to running a natural transition in the SLIP model using the hopping gait," in *Proc. Int. Conf. Robot. Biomimet.*, 2011, pp. 2163–2168.

[18] L. Visser, S. Stramigioli, and R. Carloni, "Robust bipedal walking with variable leg stiffness," in *Proc. 4th IEEE RAS EMBS Int. Conf. Biomed. Robot. Biomechatronics*, 2012, pp. 1626–1631.

[19] J. Rummel, Y. Blum, H. M. Maus, C. Rode, and A. Seyfarth, "Stable and robust walking with compliant legs," in *Proc. IEEE Int. Conf. Robot. Autom.*, 2010, pp. 5250–5255.

[20] I. Poulakakis and J. W. Grizzle, "The spring loaded inverted pendulum as the hybrid zero dynamics of an asymmetric hopper," *IEEE Trans. Automat. Control*, vol. 54, no. 8, pp. 1779–1793, Aug. 2009.

[21] D. Koepl and J. Hurst, "Force control for planar spring-mass running," in *Proc. IEEE/RSJ Int. Conf. Intell. Robots Syst.*, 2011, pp. 3758–3763.

[22] U. Saranli and D. E. Koditschek, "Template based control of hexapedal running," in *Proc. IEEE Int. Conf. Robot. Autom.*, 2003, vol. 1, pp. 1374–1379.

[23] G. Garofalo, C. Ott, and A. Albu-Schaffer, "Walking control of fully actuated robots based on the bipedal slip model," in *Proc. IEEE Int. Conf. Robot. Autom.*, 2012, pp. 1456–1463.

[24] M. M. Ankaralı and U. Saranlı, "Control of underactuated planar pronking through an embedded spring-mass Hopper template," *Auton. Robots*, vol. 30, no. 2, pp. 217–231, 2011.

[25] M. Millard, E. Kubica, and J. McPhee, "Forward dynamic human gait simulation using a SLIP target model," *Proc. IUTAM*, vol. 2, pp. 142–157, 2011.

[26] E. R. Westervelt, J. W. Grizzle, and D. E. Koditschek, "Hybrid zero dynamics of planar biped walkers," *IEEE Trans. Automat. Control*, vol. 48, no. 1, pp. 42–56, Jan. 2003.

[27] M. Shahbazi, G. Lopes, and R. Babuška, "Automated transitions between walking and running in legged robots," *IFAC Proc. Volumes*, vol. 47, no. 3, pp. 2171–2176, 2014.

[28] M. Shahbazi, R. Babuška, and G. Lopes, "Analytical approximation for the double-stance phase of a walking robot," in *Proc. IEEE Int. Conf. Robot. Autom.*, 2015, pp. 5754–5760.

[29] R. Alur *et al.*, "The algorithmic analysis of hybrid systems," *Theor. Comput. Sci.*, vol. 138, no. 1, pp. 3–34, 1995.

[30] W. J. Schwind, "Spring loaded inverted pendulum running: A plant model," Ph.D. dissertation, Dept. Elect. Eng., Syst., Univ. Michigan, Ann Arbor, MI, USA, 1998.

[31] E. T. Whittaker, *A Treatise on the Analytical Dynamics of Particles and Rigid Bodies: With an Introduction to the Problem of Three Bodies*. Cambridge, U.K.: Cambridge Univ. Press, 1970, pp. 1873–1956.

[32] P. Holmes, "Poincaré, celestial mechanics, dynamical-systems theory and chaos," *Phys. Rep.*, vol. 193, no. 3, pp. 137–163, 1990.

[33] A. Seyfarth and H. Geyer, "Natural control of spring-like running optimized self-stabilization," in *Proc. 5th Int. Conf. Climbing Walking Robots. Professional Eng. Publishing Lim.*, 2002, pp. 81–85.

[34] Y. Blum, J. Rummel, and A. Seyfarth, "Advanced swing leg control for stable locomotion," in *Proc. Autonome Mobile Systeme*, 2007, pp. 301–307.

[35] A. Seyfarth, H. Geyer, and H. Herr, "Swing-leg retraction: A simple control model for stable running," *J. Exp. Biol.*, vol. 206, no. 15, pp. 2547–2555, 2003.

[36] W. J. Schwind and D. E. Koditschek, "Approximating the stance map of a 2-DOF monoped runner," *J. Nonlinear Sci.*, vol. 10, no. 5, pp. 533–568, 2000.

[37] R. Ghigliazza, R. Altendorfer, P. Holmes, and D. Koditschek, "A simply stabilized running model," *SIAM J. Appl. Dyn. Syst.*, vol. 2, no. 2, pp. 187–218, 2003.

[38] H. Geyer, A. Seyfarth, and R. Blickhan, "Spring-mass running: Simple approximate solution and application to gait stability," *J. Theor. Biol.*, vol. 232, no. 3, pp. 315–328, 2005.

[39] J. J. Robilliard and A. M. Wilson, "Prediction of kinetics and kinematics of running animals using an analytical approximation to the planar spring-mass system," *J. Exp. Biol.*, vol. 208, no. 23, pp. 4377–4389, 2005.

[40] H. Yu, M. Li, P. Wang, and H. Cai, "Approximate perturbation stance map of the SLIP runner and application to locomotion control," *J. Bionic Eng.*, vol. 9, no. 4, pp. 411–422, 2012.

[41] O. Arslan, U. Saranli, and Ö. Morgül, "An approximate stance map of the spring mass hopper with gravity correction for nonsymmetric locomotions," in *Proc. IEEE Int. Conf. Robot. Autom.*, 2009, pp. 2388–2393.

[42] U. Saranlı, Ö. Arslan, M. M. Ankaralı, and Ö. Morgül, "Approximate analytic solutions to non-symmetric stance trajectories of the passive spring-loaded inverted pendulum with damping," *Nonlinear Dyn.*, vol. 62, no. 4, pp. 729–742, 2010.

[43] I. Uyanik, Ö. Morgül, and U. Saranli, "Experimental validation of a feed-forward predictor for the spring-loaded inverted pendulum template," *IEEE Trans. Robot.*, vol. 31, no. 1, pp. 208–216, Feb. 2015.

[44] M. M. Ankarali and U. Saranli, "Stride-to-stride energy regulation for robust self-stability of a torque-actuated dissipative spring-mass hopper," *Chaos, Interdisciplinary J. Nonlinear Sci.*, vol. 20, no. 3, 2010, Art. no. 033 121.

[45] O. Arslan, U. Saranli, and Ö. Morgül, "Reactive footstep planning for a planar spring mass hopper," in *Proc. IEEE/RSJ Int. Conf. Intell. Robots Syst.*, 2009, pp. 160–166.

[46] S. G. Carver, N. J. Cowan, and J. M. Guckenheimer, "Lateral stability of the spring-mass hopper suggests a two-step control strategy for running," *Chaos, Interdisciplinary J. Nonlinear Sci.*, vol. 19, no. 2, 2009, Art. no. 026106.

[47] G. Perdikaris, *Computer Controlled Systems: Theory and Applications* (ser. Intelligent Systems, Control and Automation: Science and Engineering). New York, NY, USA: Springer-Verlag, 1991.

[48] A. Arampatzis, G.-P. Brüggemann, and V. Metzler, "The effect of speed on leg stiffness and joint kinetics in human running," *J. Biomech.*, vol. 32, no. 12, pp. 1349–1353, 1999.

[49] K. T. Kalveram, D. F. Haeufle, A. Seyfarth, and S. Grimmer, "Energy management that generates terrain following versus apex-preserving hopping in man and machine," *Biol. Cybern.*, vol. 106, no. 1, pp. 1–13, 2012.

[50] J. E. Pratt, "Exploiting inherent robustness and natural dynamics in the control of bipedal walking robots," Ph.D. dissertation, Massachusetts Institute of Technology, Cambridge, MA, USA, 2000.

[51] D. G. Hobbelen and M. Wisse, "Controlling the walking speed in limit cycle walking," *Int. J. Robot. Res.*, vol. 27, no. 9, pp. 989–1005, 2008.

[52] J. K. Holm and M. W. Spong, "Kinetic energy shaping for gait regulation of underactuated bipeds," in *Proc. IEEE Int. Conf. Control Appl.*, 2008, pp. 1232–1238.

[53] Y. Huang *et al.*, "Step length and velocity control of a dynamic bipedal walking robot with adaptable compliant joints," *IEEE/ASME Trans. Mechatronics*, vol. 18, no. 2, pp. 598–611, Apr. 2013.

[54] T. Haarnoja, J.-L. Peralta-Cabezas, and A. Halme, "Model-based velocity control for limit cycle walking," in *Proc. IEEE/RSJ Int. Conf. Intell. Robots Syst.*, 2011, pp. 2255–2260.

[55] B. I. Prilutsky and R. J. Gregor, "Swing-and support-related muscle actions differentially trigger human walk–run and run–walk transitions," *J. Exp. Biol.*, vol. 204, no. 13, pp. 2277–2287, 2001.

[56] A. Hreljac, R. T. Imamura, R. F. Escamilla, and W. B. Edwards, "When does a gait transition occur during human locomotion," *J. Sports Sci. Med.*, vol. 6, no. 1, pp. 36–43, 2007.

[57] J. K. Hodgins, "Biped gait transitions," in *Proc. IEEE Int. Conf. Robot. Autom.*, 1991, pp. 2092–2097.

[58] C. T. Farley and O. Gonzalez, "Leg stiffness and stride frequency in human running," *J. Biomechan.*, vol. 29, no. 2, pp. 181–186, 1996.

[59] V. Segers, M. Lenoir, P. Aerts, and D. De Clercq, "Kinematics of the transition between walking and running when gradually changing speed," *Gait Posture*, vol. 26, no. 3, pp. 349–361, 2007.

[60] V. Segers, P. Aerts, M. Lenoir, and D. De Clercq, "Spatiotemporal characteristics of the walk-to-run and run-to-walk transition when gradually changing speed," *Gait Posture*, vol. 24, no. 2, pp. 247–254, 2006.
[61] H. R. Vejdani, A. Wu, H. Geyer, and J. W. Hurst, "Touch-down angle control for spring-mass walking," in *Proc. IEEE Int. Conf. Robot. Autom.*, 2015, pp. 5101–5106.
[62] Y. Liu, P. M. Wensing, D. E. Orin, and Y. F. Zheng, "Dynamic walking in a humanoid robot based on a 3D actuated dual-SLIP model," in *Proc. IEEE Int. Conf. Robot. Autom.*, 2015, pp. 5710–5717.
[63] I. Mordatch, M. De Lasa, and A. Hertzmann, "Robust physics-based locomotion using low-dimensional planning," *ACM Trans. Graph.*, vol. 29, no. 4, 2010, Art. no. 71.

Mohammad Shahbazi (M'13) received the B.Sc. and M.Sc. degrees in mechanical engineering from K. N. Toosi University of Technology, Tehran, Iran, in 2007 and 2010, respectively. He is currently working toward the Ph.D. degree in Delft Center for Systems and Control, Delft University of Technology, Delft, the Netherlands.

His research interests include nonlinear control problems for hybrid systems, robotics, and event-driven control systems.

Robert Babuška (M'15) received the M.Sc. (Hons.) degree in control engineering from Czech Technical University, Prague, Czech Republic, in 1990, and the Ph.D. (*cum laude*) degree from Delft University of Technology (TU Delft), Delft, the Netherlands, in 1997.

He has had faculty appointments with Czech Technical University in Prague and with the Electrical Engineering Faculty, TU Delft. He is currently a Professor of intelligent control and robotics in the Delft Center for Systems and Control. He is also the founding Director of the TU Delft Robotics Institute. His research interests include reinforcement learning, neural and fuzzy systems, nonlinear identification and control, state estimation, model-based and adaptive control, and dynamic multiagent systems. He has been involved in the applications of these techniques in the fields of robotics, mechatronics, and aerospace.

Gabriel A. D. Lopes (M'03) received the M.Sc. and the Ph.D. degrees in electric engineering and computer science from the University of Michigan, Ann Arbor, MI, USA, in 2003 and 2007, respectively.

He was with the GRASP Laboratory, University of Pennsylvania, Philadelphia, PA, USA, from 2005 to 2008. He is currently an Assistant Professor in the Delft Center for Systems and Control, Delft University of Technology, Delft, the Netherlands. His research interests include nonlinear control, robotics, discrete-event systems, and machine learning.